LAPPEENRANTA UNIVERSITY OF TECHNOLOGY
LUT School of Engineering Science
Degree Program in Technical Physics

Andrei Fedotov

Towards new visible light sources utilizing upconversion nanoparticles

Examiner: Professor, Erkki Lähderanta
Supervisor: Researcher, D.Sc.(Tech.), Regina Gumenyuk

ABSTRACT

Lappeenranta University of Technology
LUT School of Engineering Science
Degree Program in Technical Physics

Andrei Fedotov

Towards new visible light sources utilizing upconversion nanoparticles

Master's thesis
2017

47 pages, 33 figures

Examiners: Professor, Erkki Lähderanta
Researcher, D.Sc.(Tech.), Regina Gumenyuk

Keywords: upconversion, nanoparticles, lanthanide

This work is devoted to the study of the luminescent properties of upconversion nanoparticles and optical fibers doped with upconversion nanoparticles. The host matrices of the two types of investigated nanoparticles refer to oxides and fluorides. Both types contain Yb and Er ions, but in different concentrations. Continuous wave and pulsed pump sources of radiation at 980 and 915 nm were used for excitation of upconversion nanoparticles.

It was demonstrated that the host matrix and the concentration of lanthanide ions significantly affect the emission spectrum of upconversion nanoparticles. The degradation and saturation of luminescence in upconversion nanoparticles is revealed. The justification of these effects was proposed. In addition, the luminescence measurements of world-first optical fibers doped with upconversion nanoparticles were performed.

The results of structural studies of upconversion nanoparticles and optical fibers doped with upconversion nanoparticles using scanning and transmission electron microscopy are presented.

Acknowledgements

This work has been carried out in the Laboratory of Photonics at Tampere University of Technology. Thus, I wish to thank Pekka Savolainen for the opportunity to do my master thesis in a modern and innovative science center. I would like to express my deepest gratitude to my supervisor Regina Gumenyuk for her patience, support and guidance throughout the work. She opened a new and amazing world of photonics for me. I would like to express my highest appreciation to Professor Erkki Lähderanta for providing the opportunity to study in Finland. Especially, I wish to thank my parents Natalia and Igor for their care and support.

This work was carried out within the frame of Academy of Finland Postdoctoral Research Project (Project No. 285170).

Tampere, May 2017
Andrei Fedotov

List of abbreviations and symbols

θ_1	angle of incidence
θ_2	angle of refraction
θ_c	critical angle of incident
c	speed of light in vacuum
n	refractive index of a dielectric medium
v	phase velocity of light in a medium
α	absorption coefficient
β	propagation constant
β	propagation constant
χ	electric susceptibility
Δ	relative refractive index difference
Λ	distance between the hollows in microstructured fibers
λ_0	wavelength in vacuum
λ_g	wavelength in a waveguide
$\tilde{\mathbf{E}}$	Fourier transform of electric field $\mathbf{E}$
μ_0	magnetic constant
∇	nabla, first-order differential operator
ω	angular frequency
ϕ	angle in polar coordinate system
ρ	effective core radius

ρ	radius in polar coordinate system
$\tilde{\chi}$	Fourier transform of χ
ε_0	vacuum permittivity or electric constant
a	core radius
E_ϕ	azimuthal of the electric field in polar coordinate system
E_ρ	radial of the electric field in polar coordinate system
E_z	z-component of the electric field
H_ϕ	azimuthal of the magnetic field in polar coordinate system
H_ρ	radial of the magnetic field in polar coordinate system
H_z	z-component of the magnetic field
HE_{ml}, EH_{ml}	hybrid fiber mode
j	imaginary unit
J_m	Bessel function of the *m-th* order
k_0	free-space wave number
K_m	modified Hankel function
LP_{ml}	linearly polarized fiber mode
m	integer number
n_{eff}	effective refractive index
t	time
V	normalized frequency or V parameter
$\mathbf{B}$	magnetic flux density
$\mathbf{D}$	electric flux density
$\mathbf{E}$	electric field
$\mathbf{H}$	magnetic field
$\mathbf{M}$	magnetic polarization of the medium

P	polarization
CR	cross relaxation
CSU	cooperative sensitization upconversion
CUC	cooperative upconversion
CW	continuous wave
DC	downconversion
ESA	excited-state absorption
ETU	energy transfer upconversion
GSA	ground state absorption
MMF	multimode fiber
NIR	near-infrared
PA	photon avalanche
SEM	scanning electron microscope
SMF	single-mode fiber
TEM	transmission electron microscope
UC	upconversion
UCNPs	upconversion nanoparticles
UV	ultraviolet

Contents

1 Introduction

Sources of coherent and incoherent light are applicable in many fields, ranging from LED lamps and displays, to the creation of new materials by the laser exposure at the molecular level. Compact and inexpensive sources of visible light are in especially demand at present.

Conversion of low-energy radiation into radiation with higher energy is made possible by the use of upconversion nanoparticles (UCNPs), which represent a new class of nonlinear optical materials and have a high potential as alternative sources of visible light. Recent advances in the field of synthesis methods have led to the possibility of setting the necessary size and range of radiation of the upcoconversion nanoparticles by varying the parameters and conditions of chemical synthesis.

The upconversion nanoparticles are named because of the process that occurs in them. This phenomenon consists in the conversion of energy, which occurs due to the absorption of low-energy photons (usually from the near infrared part of spectrum) and the emission of higher-energy photons in the visible region of wavelength spectrum. Thus, the frequency of the emitted light is greater than the frequency of the exciting radiation, i.e. frequency upconversion occurs. The luminescence of the upconversion nanoparticles can be obtained using the lasers emitting in the near-infrared region.

The results of studies of the properties of such materials can find wide application in various fields. The upconversion nanoparticles attract considerable attention to the possibility of their application in lasers, medicine as biosensors, as well as in new technologies in the design of the displays and as light sources with high intensity for use in spectroscopy.

From the point of view of practical application, nanoparticle-doped fibers are a new promising direction. UCNPs embedded in a glass fiber are protected from the environment, and in addition, this approach allows to maximize the use of pumping for efficient stimulation of upconversion luminescence in the nanoparticles.

The present thesis is dedicated to this new field of nanophotonics. It describes detailed investigation of the upconversion luminescence process in nanoparticles powder and upconversion nanoparticles-doped optical fiber. The thesis consists of 7 chapters. Chapter 3 gives the necessary background about frequency conversion mechanisms. Chapter 4 is devoted to the principles of light propagation in an optical fiber. In chapter 5 experimental technique and result of luminescence measurements of UCNPs are presented. Chapter 6 describes luminescence properties of optical fibers doped with upconversion nanoparticles.

2 Nanophotonics: fundamentals and applications

Nanophotonics is a field of science that deals with the study of the interaction of light with nanoscale objects. It combines several approaches. The first way is the light confinement to the dimensions much smaller than the wavelength which is the key concept for near-field spectroscopy and microscopy. The second way is to reduce the size of objects, thus limiting the interaction between light and matter. Another approach is the nanoscale confinement of photoprocesses associated with light-induced phase change, which is the basis of the methods for the production of photonic nanostructures.

Nanomaterials are the largest part of nanophotonics. A variety of different nanostructures can be obtained within the framework of the matter confinement approach. Metal nanoparticles can serve as an example of objects with size-dependent optical properties. Electromagnetic field interacting with electrons near the metal surface causes their collective oscillations with a plasma frequency. This effect is used in the surface-enhanced Raman spectroscopy, for amplification of fluorescence and field enhancement in apertureless near-field microscopy and spectroscopy [1].

Three-dimensional confinement on the scales ranging from nanometers to tens of nanometers leads to the formation of atom-like structures called quantum dots. Similar to real atoms, they have discrete energy levels, and the distance between energy levels depends on the size of the quantum dot. Thus, it is possible to change the color of the emitted light by varying the size of the quantum dot. Currently, there are commercial technologies for producing display using quantum dots [1].

Nanostructured materials can exhibit unique nonlinear optical properties. For example, in a photonic crystal, the periodic structure of alternating regions with different refractive indices forms a photonic band gap, just as a band energy structure is formed in crystalline materials [2,3]. This feature leads to the appearance of completely new properties such as local field enhancement, microcavity effect, anomalous refractive index dispersion and anomalous group velocity dispersion which is responsible for self-collimating and extraordinary angle-sensitive light propagation and dispersion (superprism). Optical properties of the photonic crystal can find applications in low-threshold lasing, frequency conversion and optical communications [1].

Second important type of nanostructures is rare-earth-doped nanoparticles. Due to its ladder-like electronic structure, nanoparticles are able to participate in up- and downconversion processes: the absorbed near-infrared light is converted to visible radiation (upconversion) and/or to infrared radiation (downconversion). The possible use of upconversion nanoparticles lies in optical amplification, lasing and chemical sensing [1]. The present thesis is dedicated to this new field of nanophotonics. It describes detailed investigation of the upconversion luminescence process in nanoparticles powder and in UCNPs-doped optical fiber.

3 Upconversion luminescence

Electronic structure of lanthanides is ideal for converting radiation in the range from infrared to ultraviolet due to the presence of plenty of energy levels. From the viewpoint of practical application, the nanoparticles doped with elements of the lanthanide group are most convenient since they can be embedded into many photonic materials. Their energy structure is well investigated, and the synthesis process is low cost and simple. This chapter contains a description of the upconversion mechanisms, the structure and composition of UCNPs, as well as the methods for their synthesis.

3.1 Optical frequency up- and down-conversions

Definition

Most emission processes in luminescence materials are downconversion (DC) in nature, i.e. energy of emitted photon is lower than energy of absorbed photon. This effect is the result of losses due to the vibrational relaxation and known as Stokes' shift. However, for the practical application the opposite effect - upconversion (UC) emission is more interesting. Upconversion emission is a nonlinear effect where two or more near-infrared (NIR) photons are absorbed and converted into one having higher energy ranging from ultraviolet (UV) to NIR. It was first discovered in 1966 by Auzel and independently by Ovsyankin and Feofilov [4–6].

Physical mechanisms

Various mechanisms are responsible for upconversion emission and all of them can be divided into five main types: excited-state absorption (ESA) or multistep (sequential) absorption, energy transfer upconversion (ETU), cooperative sensitization upconversion (CSU), cross relaxation (CR) and photon avalanche (PA) (Fig. 1) [7].

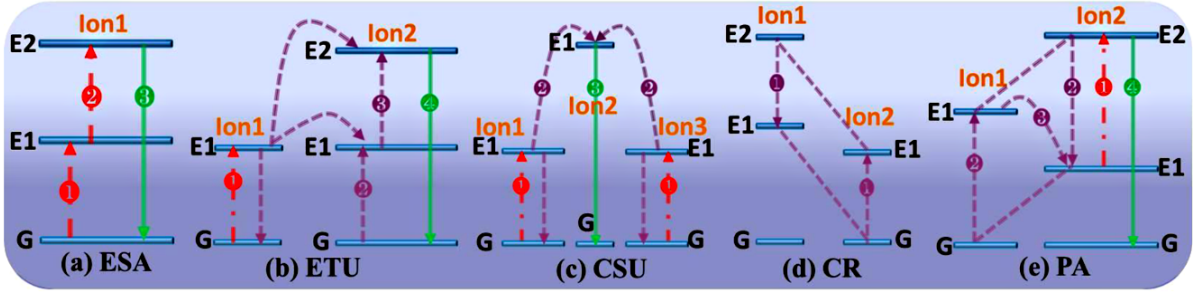

Figure 1: Upconversion mechanisms [7].

The most commonly used upconversion phosphors are the lanthanides Ln^{3+} (rare-earth) elements: Er^{3+}, Tm^{3+}, Yb^{3+}, Nd^{3+} and Pr^{3+}. Rare-earth elements are usually

ionized into trivalent state, giving off two electrons from the $6s^2$ orbitals and one electron from the $5d$ orbitals or $4f$ orbitals. Electrons located on the $4f$-shell are shielded by the outer shells $5s^2$ and $5p^6$. As a result, the position of the energy levels of the lanthanides characterized by spin-orbit interaction is very weakly depending on the environment and energy levels remains practically the same for a particular ion in different host lattices. Insensitivity to the surrounding host lattice leads to the fact that a significant number of excited f states participating in the upconversion process have sufficiently long lifetimes. Transitions between different energy levels of $4f$ orbitals occur within a particular ion. This feature and ladder-like energy structure (Fig. 2) make lanthanides ideal materials for upconversion luminescence [8].

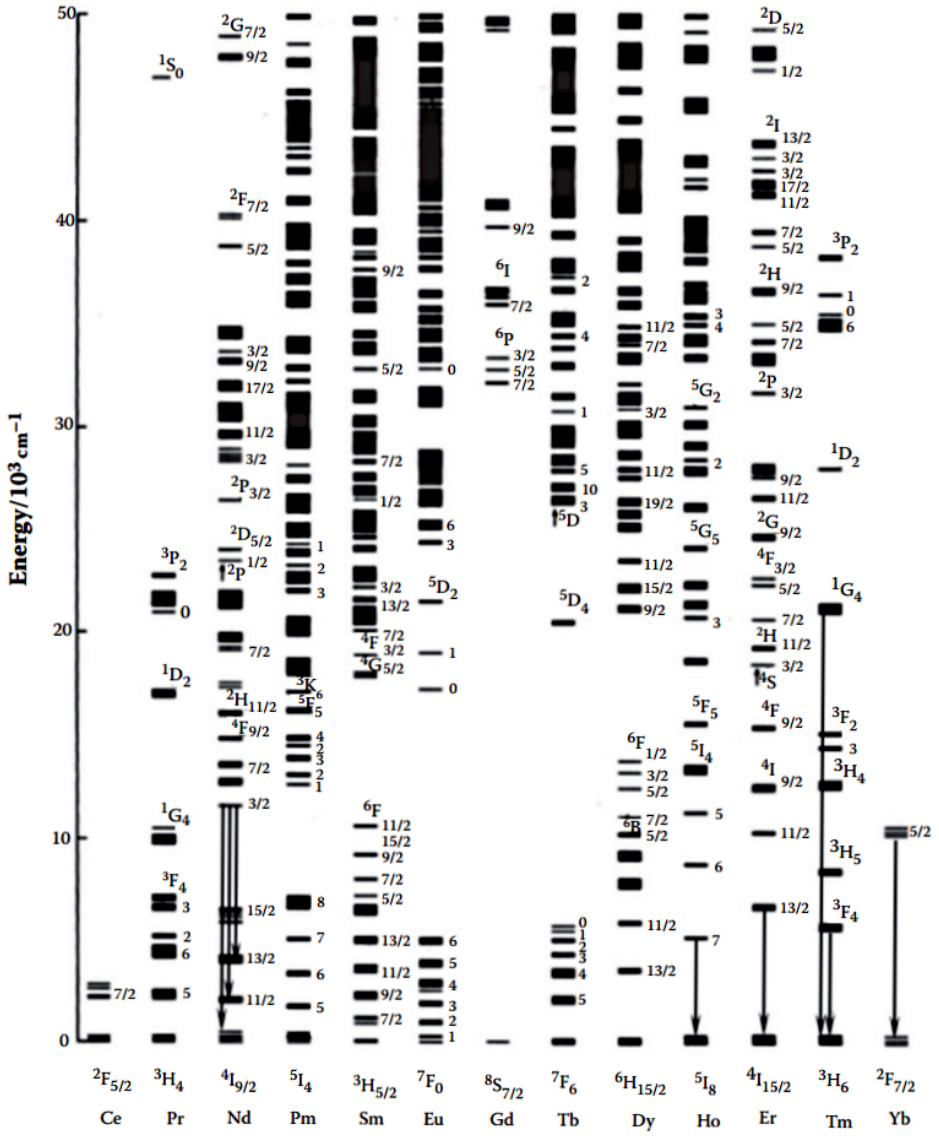

Figure 2: Energy diagram of $4f$ electrons of trivalent lanthanides [9].

Lanthanide-based upconverters consist of two components: mechanically and chemically highly stable host material with low phonon energy and rare-earth ions as

luminescence centers. Efficient luminescence is observed when host material is doped with at least two types of ions. One type, called *sensitizer*, has large effective cross section in the IR region of the spectrum. Another type has energy states with longer lifetimes and is called an *activator*. Thus, the sensitizer can non-radiatively transmit several absorbed photons to the long-lived state of the activator and excite it to higher levels. Then activator's electron decays to the ground level and emits a photon with a higher energy, which corresponds to the visible wavelength range. Usually Yb^{3+} plays the role of a sensitizer, while Tm^{3+} or Er^{3+} acts as an activator.

Excited-state absorption (ESA) is a process of sequential absorption of pump photons by a single Ln^{3+} ion. The energy diagram of ESA mechanism is a three-level structure in which the distance between the energy states G-E_1 and E_1-E_2 is the same (Fig. 1a). In an ESA process, which is termed ground state absorption (GSA), first photon excites ion from the ground state G to the intermediate level E_1, then a second similar photon promotes it to the higher E_2 state. Finally, ion decays from the excited state E_3 to the ground state G emitting photon whose energy is equal to the difference between the levels E_3 and G. Since ESA is a single-ion mechanism, the concentration of the dopants does not affect its efficiency [7].

In the case of **energy transfer upconversion** (ETU), two neighboring ions sequentially absorb pump photons. Ion 1, called the sensitizer, first absorbs the excitation photon and goes from the ground state to the metastable level E_1 (Fig. 1b). A short time later it relaxes back to the ground level and transfers its energy to ion 2, known as the activator. Thus, the ion 2 can be successively excited first to the level E_1 and then to the emitting state E_2. The efficiency of such process depends on the concentration of dopants, which affects the average distance between neighboring sensitizer-activator. Currently, the ETU is the most commonly used upconversion mechanism.

Cooperative sensitization upconversion (CSU) takes the form of interaction of three ions, two of which are usually of the same type. After absorbing pump photons, ion 1 and 3 are excited to the higher energy level E_1 (Fig. 1c). Then both of them can simultaneously transfer their extra energy to the ion 2 and return to the ground state. In that way ion 2 obtains enough energy to occupy a level higher than excited states of ion 1 and ion 3. Right afterwards ion 2 emits upconversion photon relaxing back to its ground state. Since CSU requires quasi-virtual pair levels, which are described in the theory of quantum mechanics by a higher order perturbation, as a rule its efficiency is order of magnitude lower than ESA or ETU processes [7].

When the ion relaxes to the lower state, instead of emitting a photon, it can transfer some of its energy to another ion and excite it (Fig. 1d). In this case, it does not matter what types of interacting ions. Such process is a fundamental result of ion-ion

interaction and called **cross relaxation** (CR). CR leads to well-known "concentration quenching mechanism", however it can be used to adjust color of light emitted by UPNPs. Efficiency of CR process strongly depends on dopant concentration [7].

Photon avalanche (PA) is one more upconversion mechanism discovered by Chivian and coworkers [10]. It manifests itself when the pump power reaches a certain limit. Below the threshold, fluorescence is small, but above some pumping level its intensity increases by orders of magnitude. PA includes ESA process leading to light excitation of the ion and CR providing feedback. Initially, ion 2 is excited to level E_1 in some way and may be further promoted by resonant ESA process to radiative level E_2, from which it can relax by emitting photon (Fig. 1e). However, ion 2 may also non-radiatively decay from level 2 to level 1 and transfer some of its energy to nearby ion 1. In this situation, due to the efficient CR process both ion 1 and ion 2 occupy the intermediate level E1. As a result, these two ions are ready to populate the level E_2 and further excite two another ions or participate in upconversion luminescence. The number of ions populating the energy state E_1 in such a process grows exponentially. At low pump power, low population of level 1 leads to low efficiency of ESA and CR process is negligible. The pumping intensity above the threshold produces a high population of level 2 and, consequently, through the relaxation process to a high population of level 1 leading to strong and effective upconversion fluorescence as an avalanche process [11].

3.2 Upconversion nanoparticles

Lanthanide-doped nanoparticles

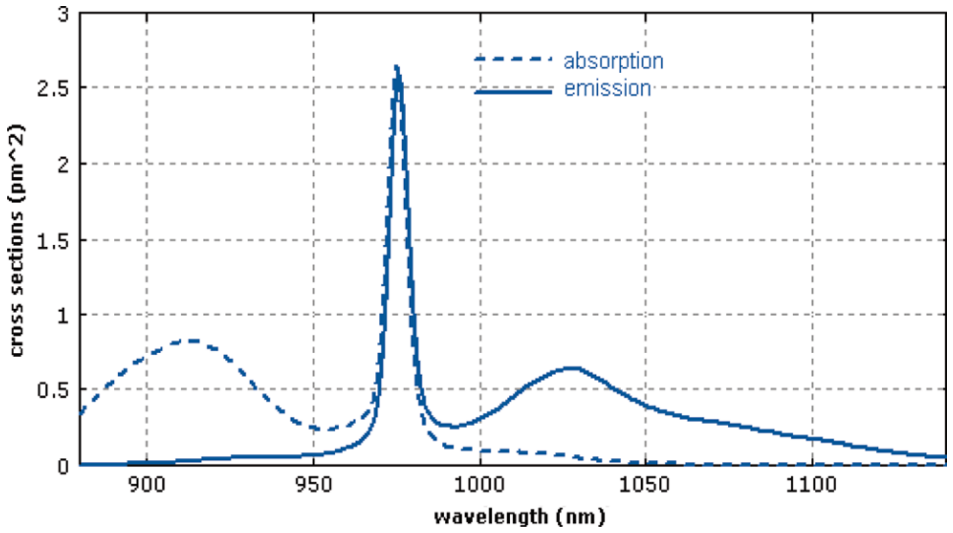

Figure 3: Absorption (dashed) and emission (solid) spectra of Yb^{3+} ions [12].

Usually, the upconversion materials consist of two components, a host matrix and doping ions. The development of new upconversion materials includes two

stages: variation of the host material and selection of the optimal concentration of doping ions. Improperly selected host lattice can increase non-radiative relaxation and, thus, significantly reduce upconversion efficiency. As mentioned above, some of the upconversion mechanisms are sensitive to ion concentration, so a too low concentration of rare-earth ions leads to ineffectiveness of these mechanisms, while too high concentration causes concentration quenching [13, 14].

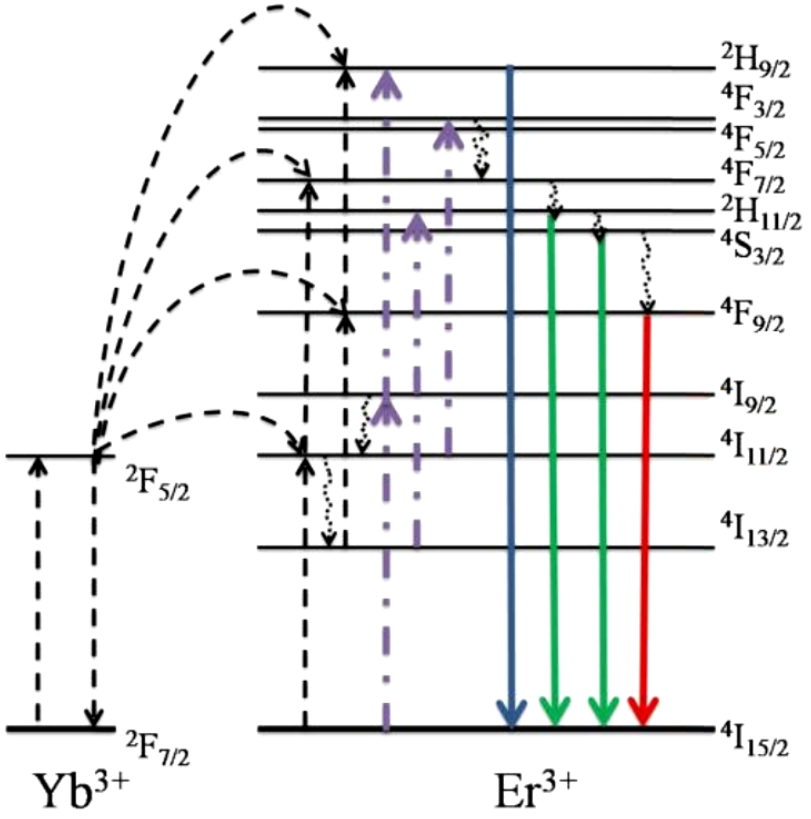

Figure 4: Schematic energy diagram of Yb^{3+} and Er^{3+} ions. Dashed arrows indicate energy transfer from sensitizer (Yb^{3+}) to activator (Er^{3+}) [15].

An upconversion compound $NaYF_4$:Yb^{3+},Er^{3+} was firstly synthesized in 1972 [16]. But only very recently it was discovered that co-doped $NaYF_4$:Yb^{3+},Er^{3+} and $NaYF_4$:Yb^{3+},Tm^{3+} have very high upconversion efficiency [17]. Therefore, this material is most often used for the synthesis of UCNPs. Yb^{3+} ions play the role of sensitizers that absorb infrared radiation (Fig. 3) and then non-radiatively transfer extra energy to Er^{3+} or Tm^{3+} ions, which act as activators producing visible or ultraviolet upconversion luminescence (Fig. 4). At the moment, $NaYF_4$ is the most efficient material for upconversion nanoparticles. Firstly, it contains Na^+ and Y^+ cations whose ionic radius is close to those of the lanthanide ions. This prevents the formation of lattice strains and crystal defects [18]. Secondly, fluorine compounds possess a chemical stability and low phonon energy ($\sim$350 cm^{-1}) [8].

The typical size of upconverison nanoparticles can vary from several nm up to 50

nm. The shape and the size strongly depend on the synthesis process and affect on the optical properties of UCNPs.

Synthesis

UCNPs can be produced in many different ways and each approach has its own application domain, taking into account advantages and disadvantages. The most commonly used techniques are coprecipitation, thermolysis, solvo(hydro)thermal process, sol-gel, combustion and method using ionic liquids.

Lanthanide-doped nanoparticles such as $NaYF_4$:Ln^{3+} are often prepared by thermolysis. This process ensures high quality of nanocrystals, monodispersion and allows controlling photoluminescent properties and sizes of nanoparticles. Thermolysis involves heating of lanthanide trifluoroacetate precorsor $(CF_3COO)_3Ln$ prepared from acid and corresponding lanthanide oxide, the addition of sodium trifluoroacetate CF_3COONa and then dropwise transferring the resulting mixture to a solution of octadecene and oleic acid. Obtained nanoparticles are percipitated by the addition of excess ethanol and are separated from the solution via centrifugation. Oleic acid acting as a surfactant controls the size of nanoparticles and prevents their aggregation by virtue of long hydrocarbon chains. Synthesis is carried out in an anhydrous and oxygen-free atmosphere [19].

Optical properties

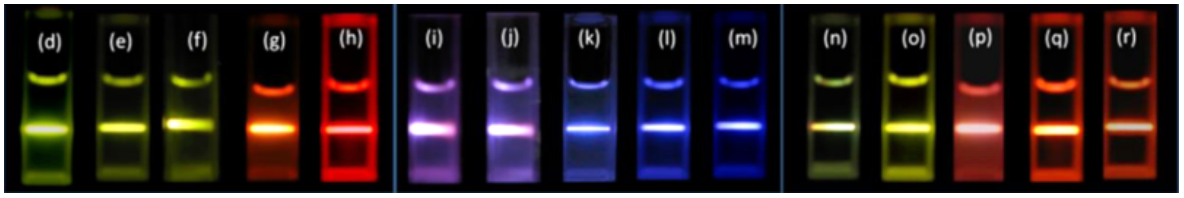

Figure 5: Photos of upconversion luminescence of colloidal nanoparticles of YF_3 doped with (d-h) Er^{3+} ions of 0.5% and Yb^{3+} ions of 10-90%; (i-m) Tm^{3+} ions of 2% and Yb^{3+} ions of 10-90%; (n-r) Er^{3+} ions of 0.5%, Tm^{3+} ions of 2%, and Yb^{3+} ions of 10-90% [20].

Upconversion nanoparticles possess strong absorption at 980 nm due to the presence of ytterbium. Depending on the nanoparticles size, shape, the dopant concentrations, surface capping ligands and other parameters, the emitted light can vary from ultraviolet to near-infrared (Fig. 5), covering the whole visible wavelength range. However, the host material has very little effect on luminescence spectra due to weak coupling of the f-f transition with the local crystal field of the host lattice, but may strongly affect on the efficiency of upconversion process. The main requirements to the host material are lattice structure compatible with rare-earth ions and low phonon energy. UCNPs can be either single color or multicolor [8].

4 Optical fibers

This chapter describes the propagation of light in an optical fiber within the framework of the basic ray theory. The concept of mode is introduced through the descriptions of the theory of electromagnetic waves in a medium. Various types of optical fibers such as single-mode, multimode and coreless fibers are described.

4.1 Basic principles of light propagation in optical fibers

Basic ray theory

In general, light wave propagates in an optical waveguide in a zigzag fashion, undergoing total internal reflections (TIR) (Fig. 6). As light is confined within an optical fiber, it is protected from external influence and passes through a fiber with low attenuation.

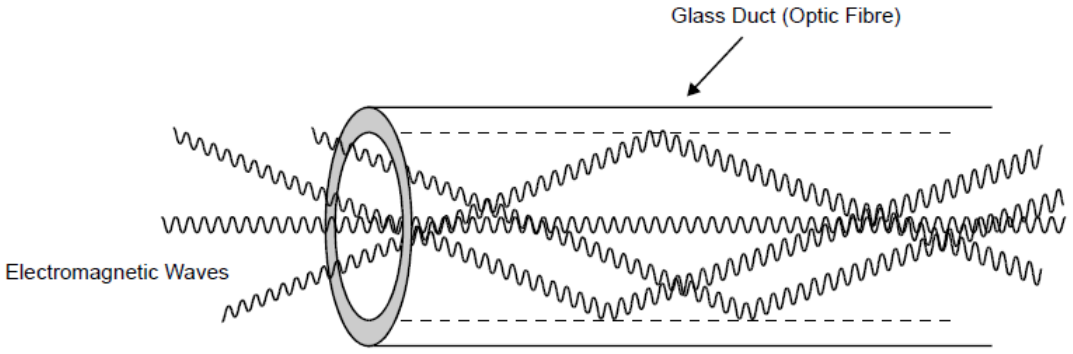

Figure 6: The propagation of electromagnetic waves in an optical fiber [21].

In order to describe the propagation of light in a waveguide using the ray theory model, it is necessary to introduce the refractive index of a material. The refractive index of the dielectric medium is a dimensionless ratio of the speed of light in vacuum to the phase velocity of light in the medium:

$$n = \frac{c}{v} \tag{4.1}$$

The more optically dense medium, the slower light travels in it, and the refractive index indicates how many times the speed of light in the material is less than in vacuum. Therefore, the denser material has the higher the refractive index. When a ray passes through the interface between two media with different refractive indices, refraction occurs. In addition, a small amount of incident light is reflected back. If a ray travels from a dielectric with higher refractive index n_1 at an angle θ_1 to the normal, then in

a medium with lower refractive index n_2 the ray will travel at an angle θ_2, where θ_2 is greater than θ_1 (Fig. 7).

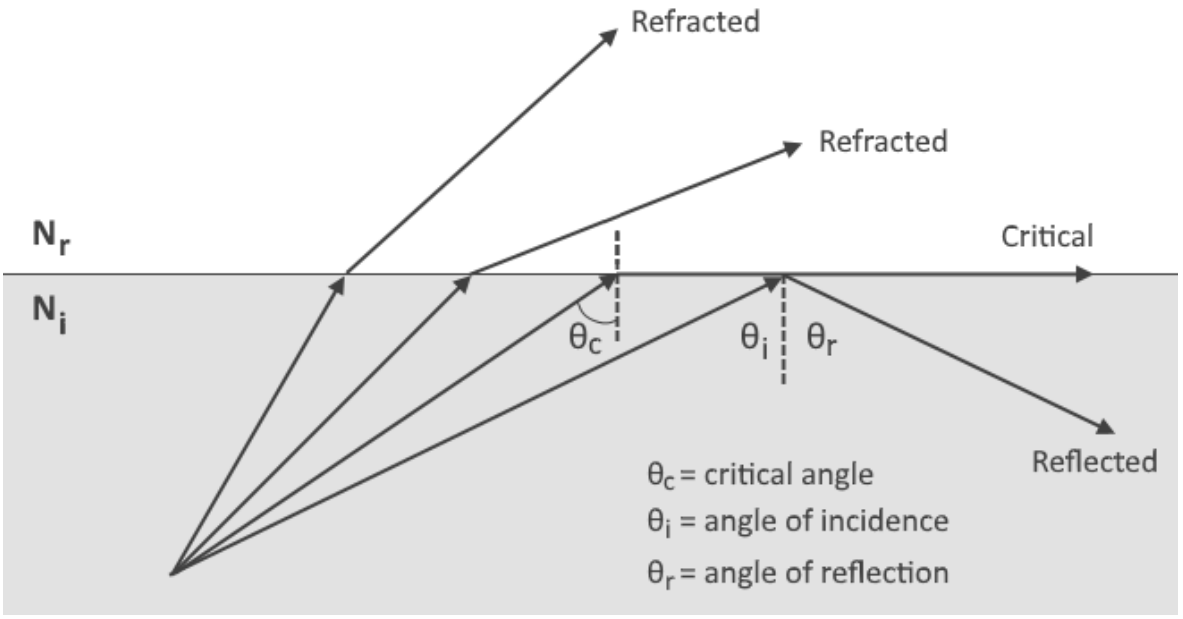

Figure 7: Illustration of ray refraction.

The refractive indices and the angles of incidence are related to each other according to Snell's law [22], which is expressed as follows

$$\frac{\sin\theta_1}{\sin\theta_2} = \frac{v_1}{v_2} = \frac{n_2}{n_1} \tag{4.2}$$

It states that the ratio of the sines of angles of the incident and refracted rays is equal to the ratio of phase velocities of these rays, or equal to the inverse ratio of the refractive indices. One can see that the angle of refraction θ_2 is always greater than the angle of incidence θ_1, since n_1 is always greater than n_2. At a certain angle of incidence θ_c, angle of refraction θ_2 will be equal to 90° (Fig. 7). In this limiting case, the critical angle of incidence θ_c can be found using the formula 4.2

$$\theta_c = \arcsin\left(\frac{n_2}{n_1}\right) \tag{4.3}$$

If rays are incident at an angle greater than critical angle, then almost all of them (99.9%) reflect back into the originating medium, i.e. they undergo total internal reflection at the interface between two dielectric materials with different refractive indices [21]. Due to this effect light in the waveguide can propagate with very low losses. Figure 8 shows the propagation of a meridional light ray along the axis of an optical fiber by means of consecutive total internal reflections at the interface of high-index core and low-index cladding.

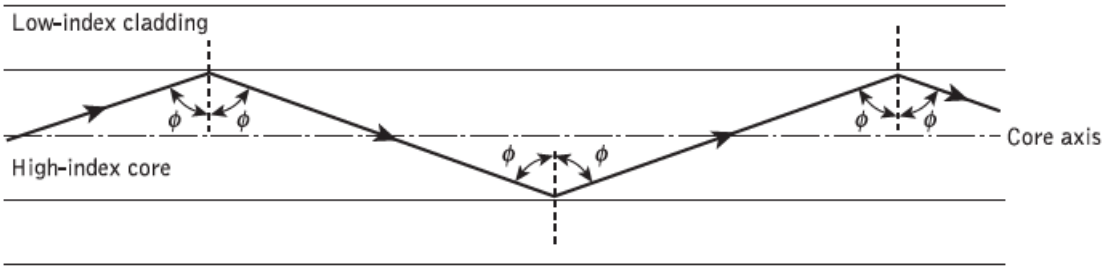

Figure 8: The light ray propagation in an ideal optical fiber [22].

In its most general form, an optical fiber consists of a core of circular section, cladding surrounding it and protective coating (jacket). To achieve total internal reflection the refractive index of a core must be higher than the outer layer. Since the air has a refractive index less than that of glass, so in this case, the light can propagate along the core even without the cladding. But in practice such implementation is not applicable because of the attenuation of the light beam caused by contamination and scratches, which cover an unprotected core.

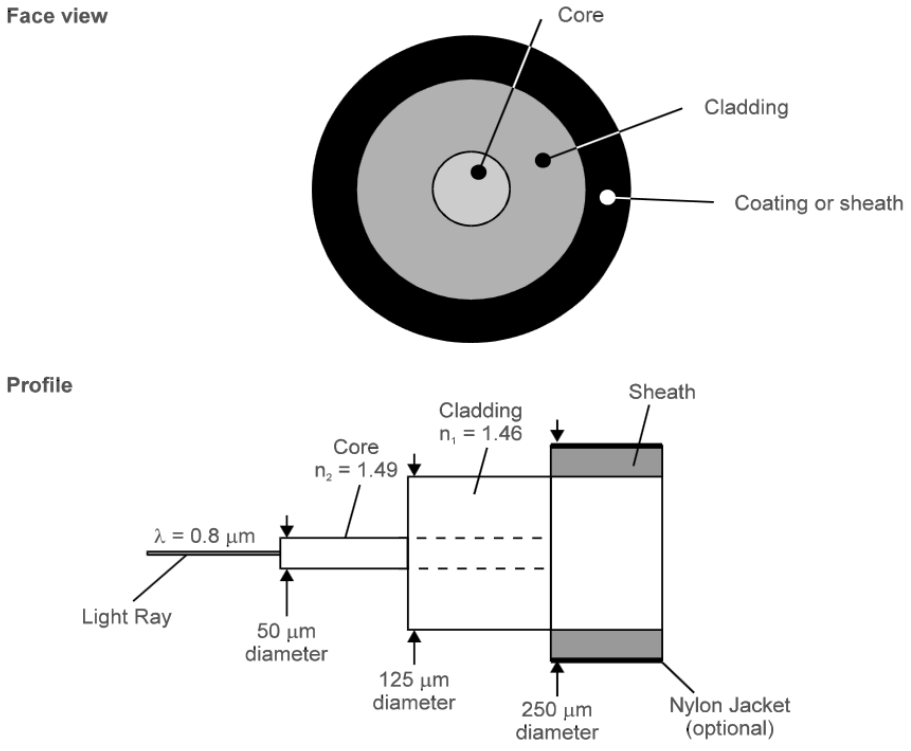

Figure 9: Face view and profile of an optical fiber [21].

Figure 9 shows the optical fiber in two projections, indicated dimensions and refractive indices are typical for the most commonly used fibers [21].

Electromagnetic mode theory

Simple ray theory described above makes it possible to understand the basic principles of light transmission in optical fibers. But in order to build a more complete model, it is necessary to consider the theory of electromagnetic waves in the medium, which is based on Maxwell's equations. For a non-conducting silica optical fiber without free charges, these equations in terms of the electric field **E**, magnetic field **H**, electric flux density **D** and magnetic flux density **B** are as follows

$$\nabla \times \mathbf{E} = -\frac{\partial \mathbf{B}}{\partial t} \tag{4.4}$$

$$\nabla \times \mathbf{H} = \frac{\partial \mathbf{D}}{\partial t} \tag{4.5}$$

$$\nabla \cdot \mathbf{D} = 0 \tag{4.6}$$

$$\nabla \cdot \mathbf{B} = 0 \tag{4.7}$$

In an external electric field **E** silica optical fiber like any other dielectric medium has an induced polarization **P**. Silica glass is an isotropic medium, so **P** is linearly proportional to **E** and can be expressed as

$$\mathbf{P} = \varepsilon_0 \cdot \chi \mathbf{E} \tag{4.8}$$

where χ is the electric susceptibility.

The flux densities and the field vectors are related by following expressions

$$\mathbf{D} = \varepsilon_0 \mathbf{E} + \mathbf{P} \tag{4.9}$$

$$\mathbf{B} = \mu_0 \mathbf{H} + \mathbf{M} \tag{4.10}$$

where ε_0 is the vacuum permittivity or electric constant, μ_0 is the magnetic constant and **M** is the magnetic polarization of the medium.

Taking the curl of Eq.4.4 and using Eqs.4.5, 4.9 and 4.10 one obtains the wave equation

$$\nabla \times \nabla \times \mathbf{E} = -\frac{1}{c^2}\frac{\partial^2 \mathbf{E}}{\partial t^2} - \mu_0 \frac{\partial^2 \mathbf{P}}{\partial t^2} \tag{4.11}$$

Using Fourier transform of $\mathbf{E}(\mathbf{r},t)$

$$\tilde{E}(\mathbf{r},\omega) = \int \mathbf{E}(\mathbf{r},\omega)\exp(j\omega t)dt \tag{4.12}$$

as well as a similar expression for $\mathbf{P}(\mathbf{r},t)$ and taking into account that $\mu_0 \cdot \varepsilon_0 = 1/c^2$, wave equation 4.11 can be written in the frequency domain as

$$\nabla \times \nabla \times \tilde{\mathbf{E}} = -\varepsilon(\mathbf{r},\omega)\frac{\omega^2}{c^2}\tilde{E}, \tag{4.13}$$

where the frequency-dependent permittivity is defined as

$$\varepsilon(\mathbf{r},\omega) = 1 + \tilde{\chi}(\mathbf{r},\omega) \tag{4.14}$$

Here $\tilde{\chi}(\mathbf{r},\omega)$ is the Fourier transform of $\chi(\mathbf{r},\omega)$ and $\tilde{\mathbf{E}}$ is Fourier transform of electric field. The frequency-dependent dielectric constant $\varepsilon(\mathbf{r},\omega)$ is a complex quantity. Its real part is responsible for the refractive index n and imaginary part is related to the absorption coefficient α

$$\varepsilon = (n + i\alpha c/2\omega)^2 \tag{4.15}$$

Hence

$$n = (1 + \mathrm{Re}\tilde{\chi})^{1/2} \tag{4.16}$$

$$\alpha = (\omega/nc)\mathrm{Im}\tilde{\chi} \tag{4.17}$$

As can be seen, both n and α are frequency dependent. After some simplifications, wave equation 4.13 takes the form

$$\nabla^2\tilde{\mathbf{E}} + n^2(\omega)k_0^2\tilde{\mathbf{E}} = 0 \tag{4.18}$$

where k_0 is the free-space wave number

$$k_0 = \omega/c = 2\pi/\lambda_0 \tag{4.19}$$

and λ_0 is the wavelength of the optical field oscillation at frequency ω in vacuum.

Mode concept

The mode concept is a main concept in the theory of light propagation in optical waveguides. An optical mode is a possible solution of Helmholtz equation (Eq. 4.20),

which is obtained from Maxwell's equations and the boundary conditions.

$$\nabla^2\mathbf{E} + n^2(\omega)k_0^2\mathbf{E} = 0 \tag{4.20}$$

Further discussion refers only to the guided modes of a step-index optical fiber.

Because of the shape of an optical fiber it makes sense to seek a solution of Eq. 4.20 in the cylindrical coordinates with z-axis directed along the axis of the fiber. Solution can be found by method of variable separation:

$$E_z(\rho, \phi, z) = F(\rho)\Phi(\phi)Z(z) \tag{4.21}$$

Here this method is applied only for longitudinal component E_z of the electric field vector. Other components of electromagnetic field ($E_\rho,\ E_\phi,\ H_\rho,\ H_\phi,\ H_z$) can be expressed using Maxwell's equation. When all variables in Eq.4.21 are found, the general solution of Eq.4.20 has the form

$$E_z = \begin{cases} AJ_m(p\rho)\exp(jm\phi)\exp(j\beta z), & \rho \leq a \\ CK_m(q\rho)\exp(jm\phi)\exp(j\beta z), & \rho > a \end{cases} \tag{4.22}$$

where A, C are constants, $J_m,\ K_m$ are Bessel and modified Hankel functions, a is the radius of fiber core and $p,\ q$ parameters are defined in a following way

$$p^2 = n_1^2k_0^2 - \beta^2 \tag{4.23}$$

$$q^2 = \beta^2 - n_2^2k_0^2 \tag{4.24}$$

Similar solution for longitudinal component H_z is

$$H_z = \begin{cases} BJ_m(p\rho)\exp(jm\phi)\exp(j\beta z), & \rho \leq a \\ DK_m(q\rho)\exp(jm\phi)\exp(j\beta z), & \rho > a \end{cases} \tag{4.25}$$

where m is an integer number.

In an optical fiber both components E_z and H_z are nonzero ($m = 0$ is exception). Therefore, fiber modes are hybrid modes and denoted by EH_{ml} or HE_{ml}, depending on whether E_z or H_z dominates. For weakly guiding fibers another notation LP_{ml} (linearly polarized modes) is used.

Propagation constant β uniquely determines a fiber mode, which propagates with an effective refractive index $n_{eff} = \beta/k_0$. Its value lies in the range $n_1 > \bar{n} > n_2$. Similar to the bulk refractive index, the effective refractive index changes the wavelength in

the waveguide as follows

$$\lambda_g = \lambda_0 / n_{eff} \tag{4.26}$$

Inside the cladding the optical field decays exponentially. It does not occur until $n_{eff} < n_2$. But when $q^2 = \beta^2 - n_2^2 k_0^2 = 0$ or $n_{eff} = n_2$, the mode reach cutoff, meaning that a single-mode regime is established.

The normalized frequency or V parameter is defined as

$$V = k_0 a (n_1^2 - n_2^2)^{1/2} \approx (2\pi/\lambda) a n_1 \sqrt{2\Delta} \tag{4.27}$$

This quantity is useful to express cutoff condition through the refractive indices of core n_1 and cladding n_2, core radius a and wavelength λ of light propagating in a fiber [23, 24].

For large values of V, fiber supports propagation of many modes. Starting from a certain value of V only single-mode operation is possible. Thus, all optical fibers with glass cladding surrounding can be divided into two large groups: single-mode and multi-mode fibers. The term multi-mode is usually applied to the fibers with a core diameter of 50 microns or more. Due to the relatively large core diameter, multiple modes of light propagate in such a fiber [21].

4.2 Types of optical fibers

Single- and multimode fiber

An optical fiber consists of a glass core with an uniform refractive index and a circular cross section, surrounded by cladding with a slightly lower refractive index. Figure 10a and 10b shows profile of single-mode and multimode fiber having an abrupt change at the core-cladding boundary. When light propagates inside a multimode fiber (MMF), it undergoes multiple total internal reflections from the core-cladding interface and travels in zig-zag manner inside the core.

The diameter of the core in a single-mode fiber (SMF) is from 2 to 10 μm. This allows the propagation of only one transverse mode. The single-mode fiber is free from intermodal dispersion (light pulse broadening). Typical diameter of a multimode fiber is 50 μm or greater, which leads to the propagation of many modes inside the core [22]. The fiber may also not have a core (Fig. 10c). Then air play the role of the shell with a smaller refractive index. Such a fiber is called coreless. It is easier to manufacture and usually they are used for testing of doping technology.

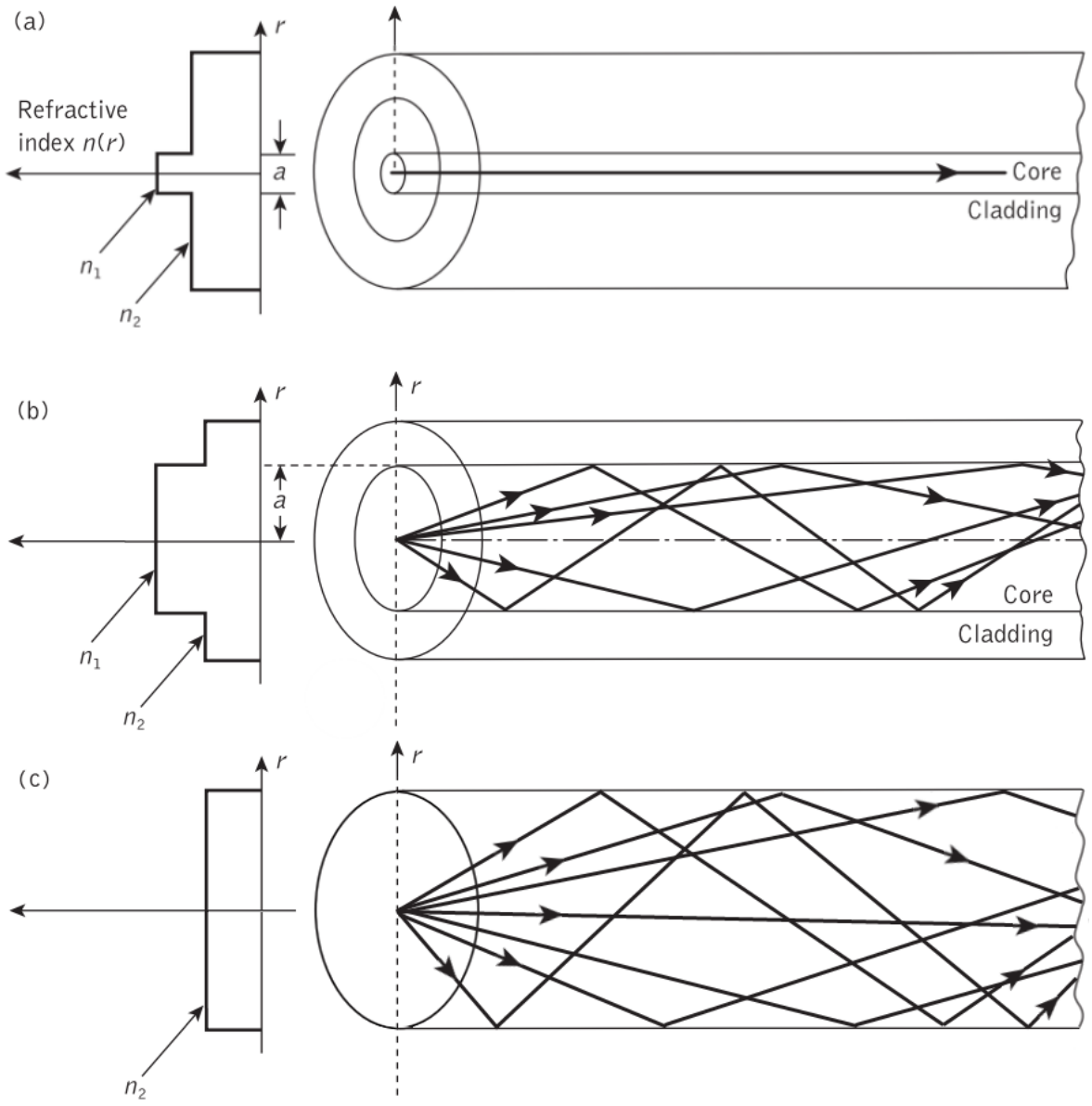

Figure 10: The refractive index profile and ray propagation in (a) single-mode, (b) multimode, (c) coreless fiber [22].

4.3 Rare-earth-doped fibers

Rare-earth-doped fibers are optical fibers, the core of which contains embedded ions of the lanthanide group. The most commonly used ions are ytterbium, erbium, thulium, niobium, holmium and europium. For practical use, the glass core matrix is doped with rare-earth elements with concentrations ranging from tens to several thousand parts per million. To achieve maximum efficiency, the doping profile should be a delta function with a maximum in the center of the core. However, it is necessary to balance the spatial confinement and concentration of rare-earth elements, since a stronger confinement requires higher concentration. In turn, too strong concentration leads to clustering and, as a result, to fluorescence quenching and a decrease in device

performance [25].

The composition of the glass host matrix is also extremely important and primarily determines the solubility of rare-earth elements, which affects the fluorescence emission, absorption and cross section of ESA. Commercially-used fiber lasers are mainly based on a phosphate or multicomponent silicate composition, which were designed to prevent the clustering at high doping concentration [26].

4.4 Fiber glass materials

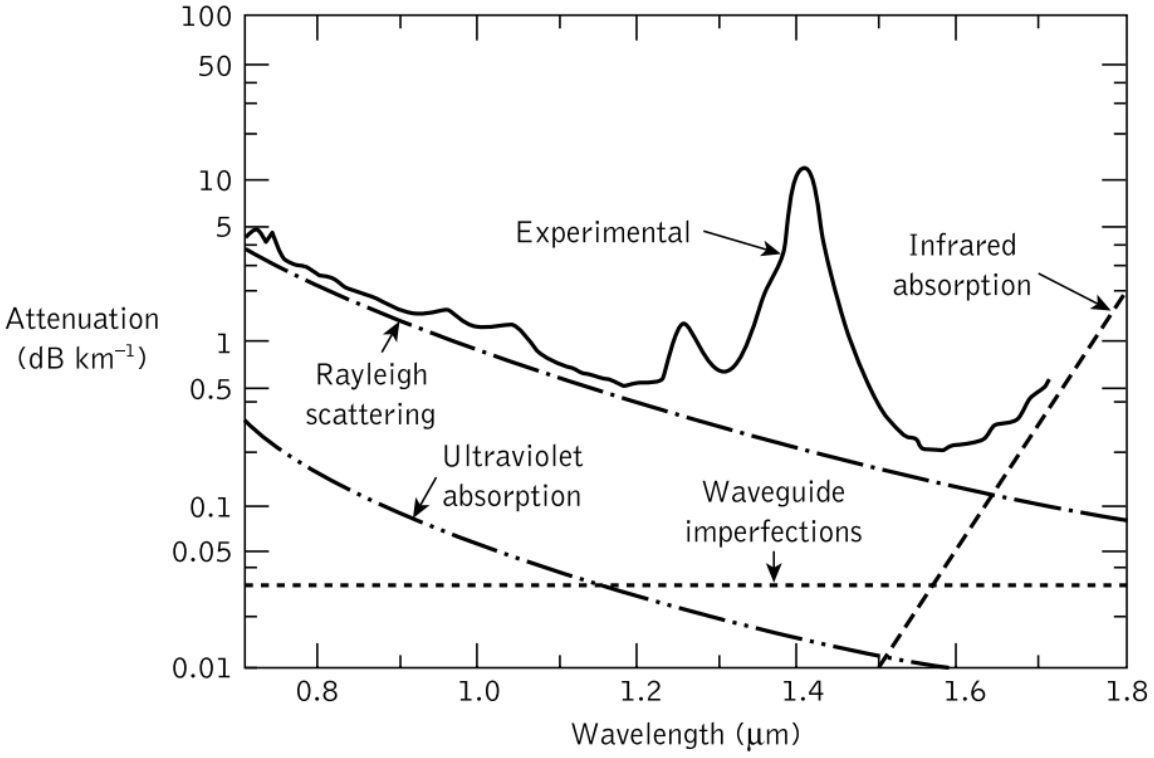

Figure 11: The measured attenuation spectrum of an ultra-low-loss silica fiber (solid line) and various attenuation mechanisms (dashed line) [22].

Most of the glass optical fibers are produced from silicon dioxide. Depending on the field of application, various chemical elements such as boron, phosphorus, germanium, tellurium and aluminium can also be added to the glass matrix. The addition of impurities affects the refractive index and phonon energy, latter is critically important in the case of fibers doped with rare-earth materials. To prevent the clustering of lanthanides, the silica fibers with sodium and aluminum are used as a host matrix. The advantage of silica-based fibers is that they are transparent in a wide spectral range. In the near infrared part of the spectrum (about 1.5 μm), they demonstrate extremely low absorption and scattering losses. However, the presence of hydroxyl (OH) groups leads to strong absorption at a wavelength of 1.4 μm (Fig. 11). At the

same time, a high concentration of OH groups reduces the absorption in the ultraviolet region [22, 27].

The disadvantage of silica fiber is high phonon energy of $\sim$1100 cm^{-1}. Therefore, tellurite (phonon energy $\sim$700 cm^{-1}) and fluoride (phonon energy $\sim$350 cm^{-1}) fibers with lower phonon energy have been developed, since the phonon-induced non-radiative relaxation is the main mechanism that negatively affects the upconversion efficiency. In addition to low phonon energy, fluoride glass is characterized by the absence of hydroxyl groups, high chemical stability and transparency from 250 nm (ultraviolet) to 2 μm wavelengths. These features make them optimal material for rare-earth doped fibers [8].

5 Characterization of nanoparticles

The luminescent properties of upconversion nanoparticles depend on many factors and one of them is host matrix composition. This chapter presents studies of the luminescence of two types of nanoparticles. Both types are doped with Yb and Er ions, but they have different host matrices. As pump sources, 980 nm and 915 nm laser diodes were used. Supercontinuum laser with a cut out and amplified portion of the spectrum at 980 nm played a role of pulse pumping.

5.1 Sources of pump light

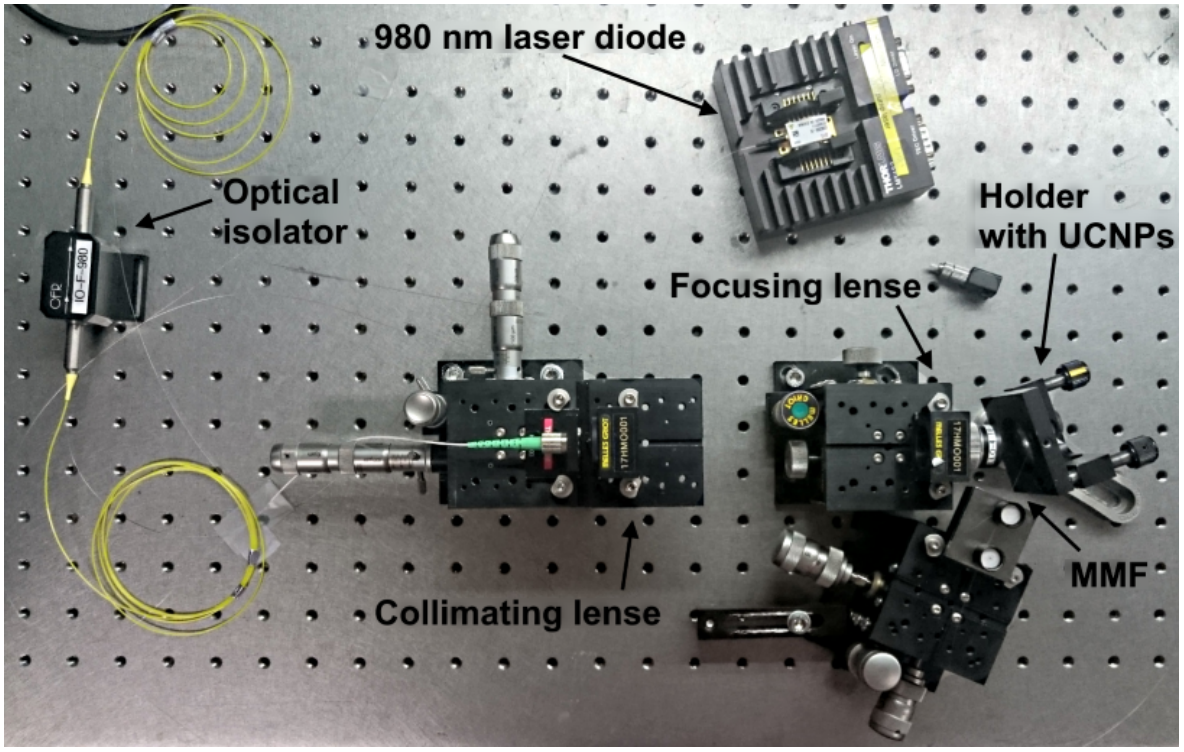

Figure 12: The scheme for measuring the luminescence of UCNPs using 980nm CW laser diode.

The setup for the measurements of upconversion luminescence spectra are shown in Fig. 12. The pump source light is delivered via a fiber pigtail. The light further collimated by the first optical lens. The second lens is used for focusing of the pump light directly on the UCNPs samples. Both lenses and fiber pigtail are placed on the optical stages. Powder of upconversion nanoparticles was attached to double-side adhesive tape and mounted on the holder (Fig. 12, 13). The UCNPs powder was irradiated with the pump beam, and after that emitted light and residual pump were collected using 105/125 μm multimode optical fiber (MMF), placed closely to the sample. The measurements of the emission spectra of the upconversion nanoparticles

were performed using Yokogawa optical spectrum analyzer.

As a pump source three options were employed: 980 nm continuous wave (CW) laser diode, 915 nm CW laser diode and 980 nm pulsed source. A continiuos wave (CW) laser diode II-VI LC96Z600-76 was chosen as a source of 980 nm light for an excitation of UCNPs. The maximum power of the laser diode is about 200 mW, at a maximum current of 800 mA. The laser diode has output single-mode fiber pigtail for light delivering. The core diameter of the output pigtail was equal to 4.4 μm surrounded by 125 µm of the cladding area. The numerical aperture (NA) of the fiber was 0.16. An optical isolator with input and output single mode fiber pigtails was spliced to the diode pigtail to prevent back reflections that could damage the pump source.

For pumping at 915 nm, laser diode K915FA3RN-25.00W (BWT Beijing Ltd.) was used. The laser beam was collimated and then focused with a lens system (Fig. 12). The laser diode delivered up to 1.1 W power launched into multi-mode output fiber pigtail with core/cladding parameters as 105/125 μm and 0.22 NA.

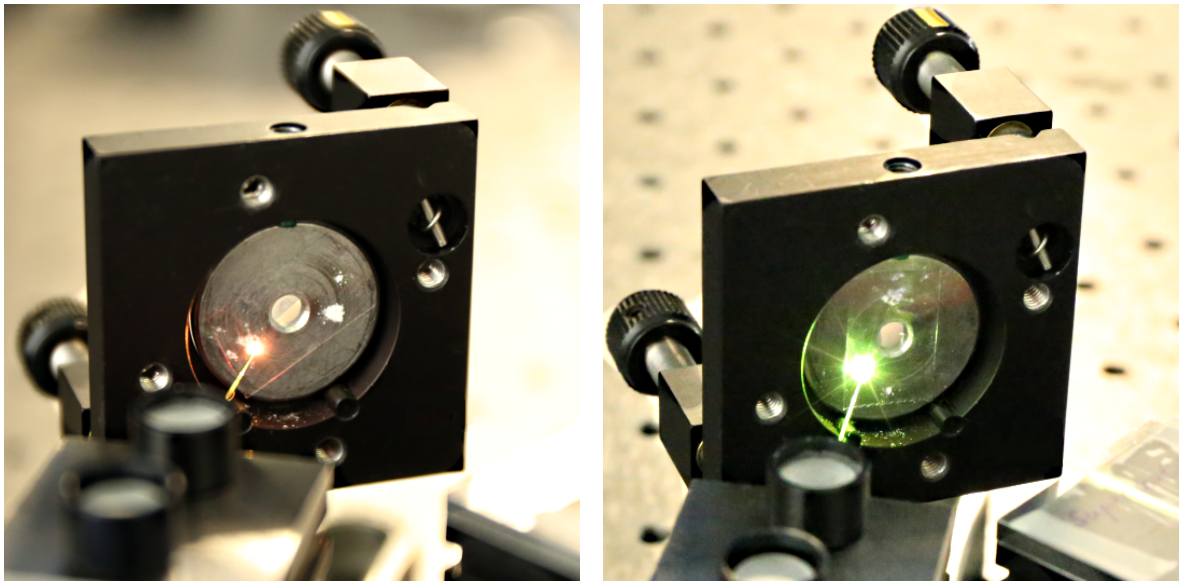

a) b)

Figure 13: Upconversion luminescence: a) Y_2O_3:Yb,Er, b) $NaYF_4$:Yb,Er UCNPs.

In order to investigate the upconversion luminescence of nanoparticles under 980 nm pulsed pumping a pulsed source of 980 nm and fiber amplifier were built up. Measurements with pumping in the pulsed mode make it possible to minimize the effects associated with the heating of the sample. Due to the short duration of the pulses of 6 ps, the material does not have time to heat up, as is the case with constant pumping.

980 nm ultra-fast pulse laser can be built up only by using Yb-doped fiber since it has emission at 980 nm under excitation by 915 nm source. However, due to high cross-section value of Yb-ions (Fig. 4) at 980 nm, there is an effect of strong light reabsorption

with further emission at 1040 nm wavelength. It means that the internal losses in the laser cavity becomes very high exceeding the gain. This fact denotes that the design of 980 nm pulse laser is a very complicated task, which separately requires a lot of efforts. Therefore, can easier solution has been found. A supercontinuum laser was used to obtain pulses at the given wavelength. Supercontinuum laser is a multi-stage fiber laser comprising several principal parts: 1) Ultra-fast pulse laser – seed. It delivers low power (couple of mW) ultra-short pulses (several ps) with fixed repetition rate (tens of MHz). 2) These pulses are further stretched in time domain and amplified in multi-stage fiber amplifier operated by chirp pulse amplification (CPA) scheme. 3) These high power long pulses are then compressed in time domain down to their transform-limited value. Now they are extremely high peak power ultra-short pulses. 4) These pulses are launched into highly nonlinear optical fiber, which generates multiple new harmonics in the broad wavelength spectrum range by stimulated nonlinear process. At the output of the source it gives a pulse of extremely broad light covered visible, near-infrared and infrared ranges.

Supercontinuum laser "Fianium" (NKT Photonics A/S) generates ultra-broadband radiation with the repetition rate of 20 MHz. It has a continuous spectrum in a range from 450 nm to beyond 2 μm, so the portion of the spectrum at a wavelength of 980 nm can be cut by the use of an interference bandpass filter. The bandpass filter FB980-10 (Thorlabs Inc.) was utilized in the setup (Fig. 14). It features a center wavelengths of 980 nm and has FWHM equal to 10 nm. After filtration 980 nm light was lauched into a single-mode fiber by means of a focusing lens with aperture compatible with fiber NA to obtain high efficiency of light coupling. The measured value of the light power at a wavelength of 980 nm in single mode fiber was about 100 μW. Since the directly obtained power from supercontinuum source is too low for stimulation of upconversion process, the 980 nm light was further amplified in Yb-doped fiber amplifier.

A bidirectional pumping scheme was chosen for fiber amplifier. In general, it consists of two counter-directed 915 nm laser diodes, active Yb-doped fiber between them and signal source of 980 nm radiation (Fig. 14). The first fiber dichroic coupler combines the input signal and pumping from 915 nm single-mode laser diode (Lumics SN0713368) which is connected in forward direction meaning that it coincides with the direction of the input signal propagation. The second 915 nm single-mode laser diode (Lumics SN0713367) emits in backward direction through the other fiber dichroic coupler, which serves to separate the backward pumping from the amplified signal. The highly concentrated ytterbium-doped phosphor-silicate fiber length of 4 centimeters acts as an active medium and converts light at 915 nm to 980 nm. The cut-off wavelength of the fiber (the transition from multi-mode to single-mode operation) is situated below 915 nm ensured efficient pump light conversion into the

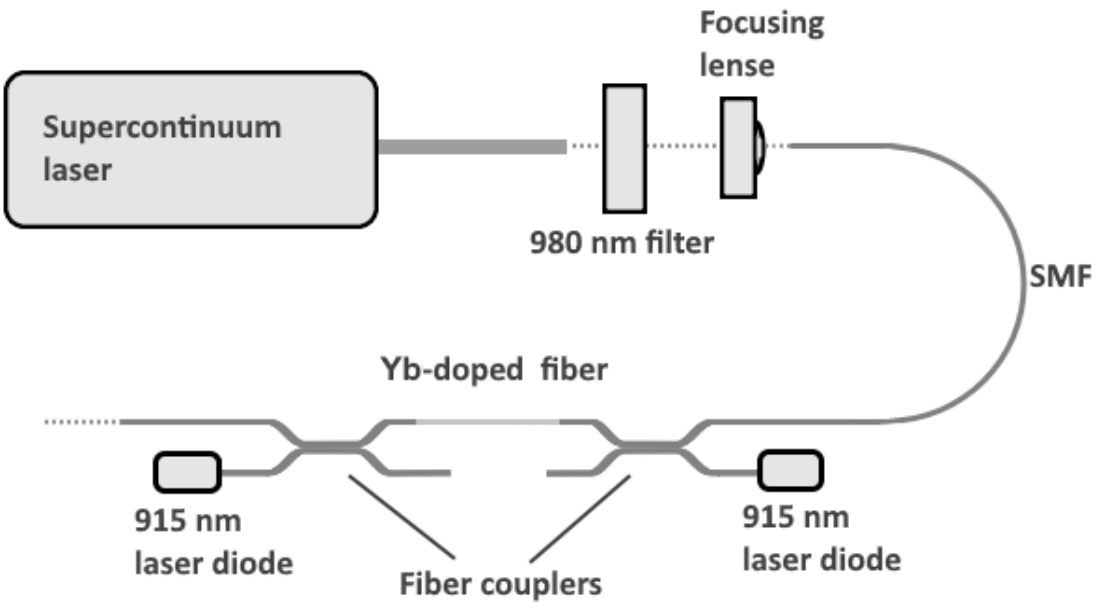

Figure 14: Scheme of bidirectional pumped fiber amplifier.

signal (pump light and signal modes are fully overlapped). The high-concentration of Yb-ions promotes the efficient amplification at 980 nm, while extremely short fiber length prevents reabsorption effect with further emission at the longer wavelength.

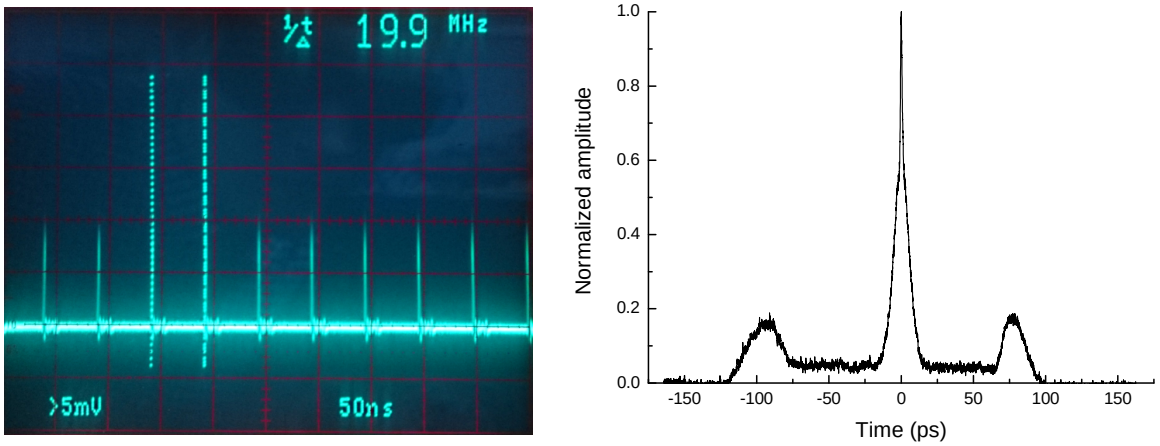

a) b)

Figure 15: Oscilloscope picture of the pulse train (a) and the autocorrelation trace of the pulse (b) after the light amplification.

As a result, the oscilloscope picture and the autocorrelation traces of the pulse obtained at the output of the Yb-doped amplifier are shown in Fig. 15. The oscilloscope picture shows pulse train with repetition rate of 20 MHz. The autocorrelation measurements reveals three peaks: the central peak and two at the side. The autocorrelation image should be discerned in the way that the number of pulses includes

the central peak and the pulses situated from one side of the central peak. The pulses on the other side of the central peak are simply the reflection of the side pulses. The amplitude of the side peaks are always lower that the central peak and decreases gradually with the increase in the pulse separation. It is a specific of autocorrelation measurement technique. Therefore, there is a pulse pair with the separation distance of approximately 100 ps. The second pulse could be generated by the seed laser of supercontinuum sources or could be a result of the pulse splitting due to the spectral filtering or amplification. The pulse duration of the central peak was equaled to 6 ps.

The forward laser diode operating alone amplifies the signal approximately by 23 dB to average power of 20 mW. Adding a backward laser diode enhances the average power of the output signal to 50 mW, that, however, leads to the appearance of a pump component at 915 nm in the amplified signal.

5.2 SEM and TEM analysis of upconversion nanoparticles

The first type of UCNPs (PTIR660/UF) was synthesized by Phosphor Technology Ltd. (Stevenage, England). Their chemical composition is Y_2O_3:Yb,Er. The percentage of lanthanides, as well as the method and parameters of the synthesis are the trade secret of the manufacturer.

The second type of UCNPs $NaYF_4$:Yb,Er was provided by University of Turku. Their composition is following: Na: 11.2, Y: 34.8, F: 37.2, Yb: 14.4 and Er: 2.4 wgt%. Nanoparticles were synthesized by the modified thermal coprecipitation method.

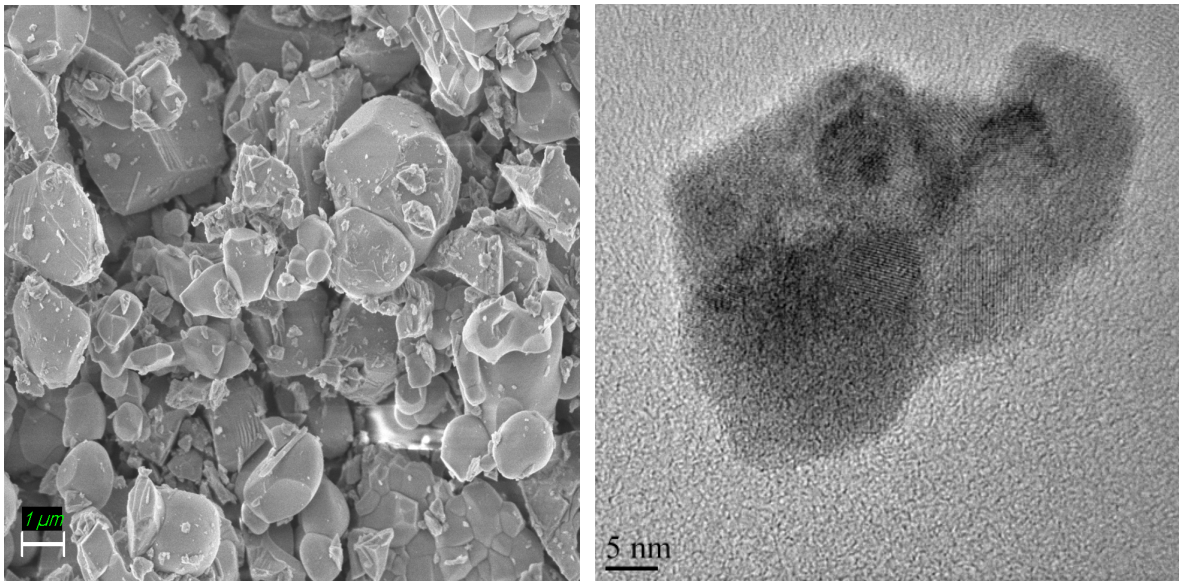

a) b)

Figure 16: SEM (a) and TEM (b) images of Y_2O_3:Yb,Er UCNPs.

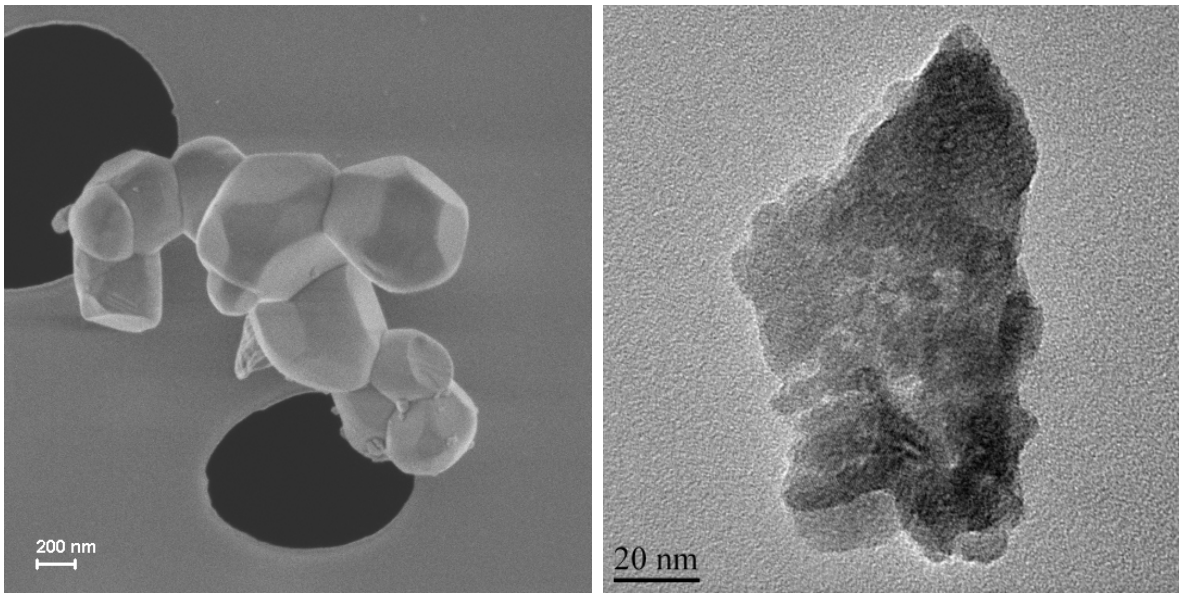

a) b)

Figure 17: SEM (a) and TEM (b) images of $NaYF_4$:Yb,Er UCNPs.

Both types of upconversion nanoparticles were examined using a scanning electron microscope (SEM) and a transmission electron microscope (TEM) to determine their shapes and sizes. The powder of the samples comprised big clusters in the range from 1 to 2 μm (Fig. 16a). The presence of micron-size clusters is due to the high ability of nanoparticles to form big agglomerates in the absence of special nanoparticles' surface treatments. As can be seen from the TEM image (Fig. 16b), regions with differently oriented crystal lattices are present in the nanoparticle. This indicates that each particle consists of smaller grains.

The single nanoparticle size of Y_2O_3:Yb,Er and $NaYF_4$:Yb,Er samples lays within the range of 10 nm (Fig. 16, 17). The shape of Y_2O_3:Yb,Er sample can be determined as round, while $NaYF_4$:Yb,Er sample characterizes by hexagonal structure.

5.3 Luminescence spectra measurements

The luminescence spectrum of Y_2O_3:Yb,Er nanoparticles obtained under 980 nm CW excitation is shown in Fig. 18. The first type of UCNPs emits at wavelengths of 523, 539 662 nm (Fig. 18). These peaks correspond to electronic transitions $^2H_{11/2}$ $\rightarrow{}^4I_{15/2}$, $^4S_{3/2}$ $\rightarrow{}^4I_{15/2}$ and $^4F_{9/2}$ $\rightarrow{}^4I_{15/2}$ (Fig. 20a), respectively [28–30].

Pumping at 980 nm easily excites the Yb^{3+} ion from $^2F_{7/2}$ level to $^2F_{5/2}$. As shown in Fig. 4, state $^2F_{5/2}$ of ytterbium and state $^4I_{11/2}$ of erbium are on the same level, therefore resonant energy transfer is possible between them. Thus, erbium can be excited to level $^4I_{11/2}$, and then through the same mechanism to level $^4F_{7/2}$. The excited Er^{3+} ion can lose some of its energy and non-radiatively relax to $^2H_{11/2}$, $^4S_{3/2}$

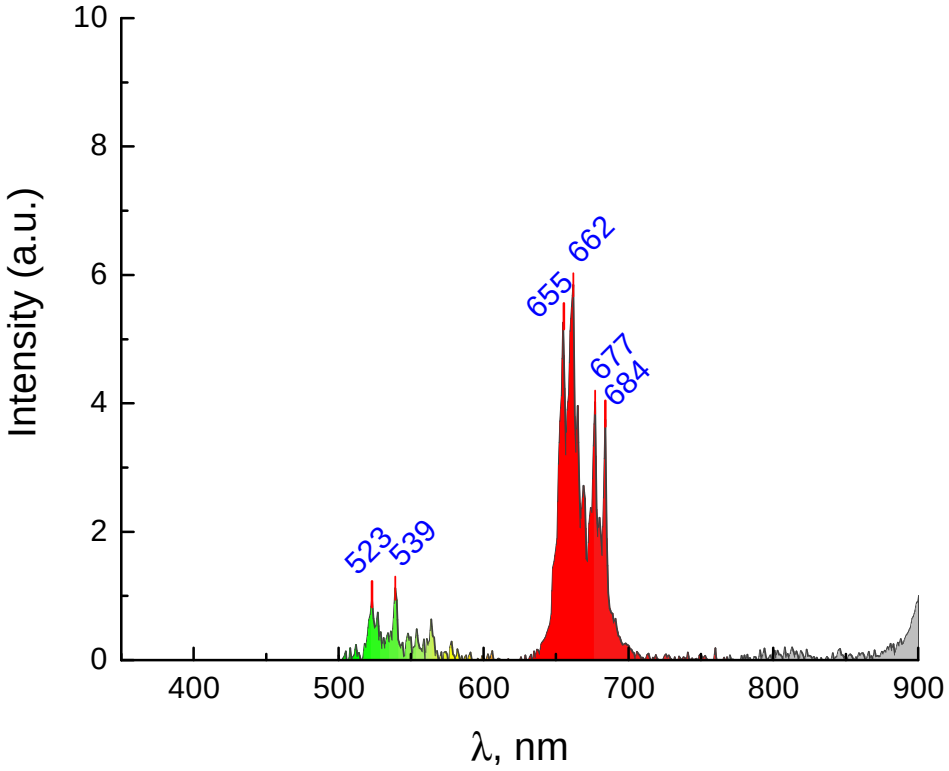

Figure 18: Spectrum of Y_2O_3:Yb,Er UCNPs within the range of 500 to 900 nm obtained under 980 nm CW pumping.

and then decay to ground level emitting photon. It is also possible that the ion relaxes immediately to level $^4I_{13/2}$ after the first energy transfer, and then is excited to level $^4F_{9/2}$, the transition from which to the ground state corresponds to a photon with a wavelength of 662 nm. Both red and green emissions require the sequential absorption of two photons. However fluorescence of these nanoparticles is stronger at red wavelength (Fig. 13a), but the spectrum has a small peak also at green wavelength. Therefore, they can be specified as a source of bicolor light.

Besides the peaks at 523, 539 and 662 nm, demonstrated by the first type of UCNPs, $NaYF_4$:Yb,Er the UCNPs have peaks also in violet (377, 408), blue (487), green (528, 541, 551), red (654) and infrared (840) portion of the spectrum (Fig. 19). Therefore, they can serve as a source of white light. Since it was recently announced that population inversion has been achieved in UCNPs [31], they can potentially compete with the supercontinuum lasers. All these peaks correspond also to the previously calculated Er^{3+} energy levels (Fig. 20) [28–30]. In addition to the transitions described for the first type of nanoparticles, transitions from levels $^4F_{7/2}$, $^2H_{9/2}$, $^4G_{11/2}$ to the ground state are also possible for these nanoparticles. Since the emission in the violet region requires sequential absorption of three photons, therefore the intensity of the corresponding peaks in the spectrum is low.

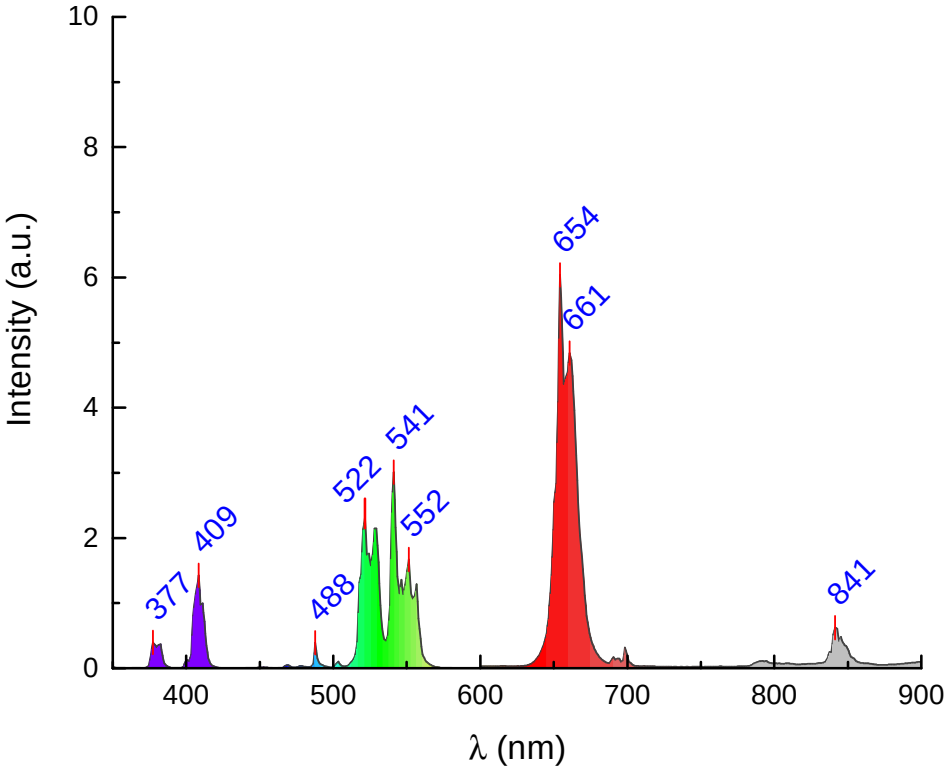

Figure 19: Spectrum of $NaYF_4$:Yb,Er UCNPs within the range of 350 to 900 nm obtained under 980 nm CW pumping.

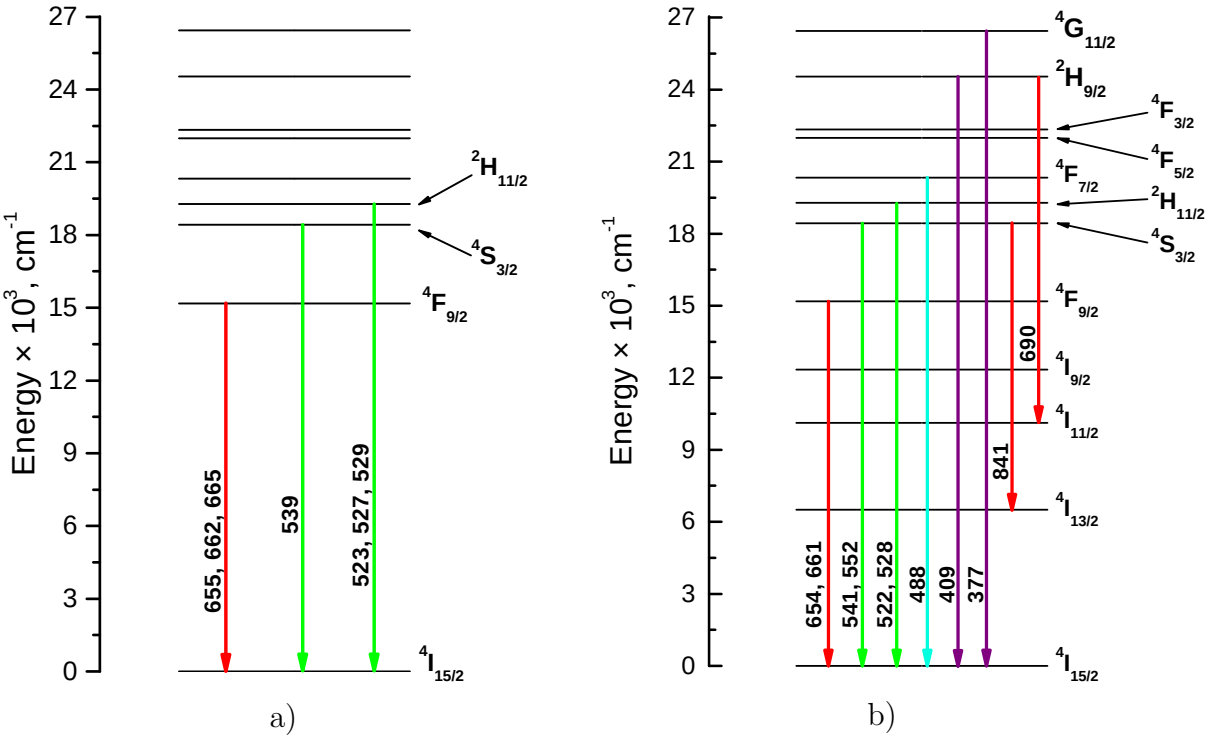

Figure 20: Upconversion luminescence: a) Y_2O_3:Yb,Er, b) $NaYF_4$:Yb,Er UCNPs.

In addition, the dependence of luminescence intensity on pump power density was obtained for each type of nanoparticles. The luminescence intensity was determined by integration of the peaks on the spectra, which was obtained for pump power densities. The calculated dependence for the first type of nanoparticles is presented in Fig. 21. At low pump power density it demonstrates the grow of upconversion luminescence, and reaches its maximum values at intensity of pump light of 200 kW/cm^2. A further increase of pump power density leads to saturation of the upconversion effect. When the pump power density exceeds the value of 220 kW/cm^2, the luminescence intensity strongly decreases approaching the initial values. It denotes the upconversion degradation at high pump power density.

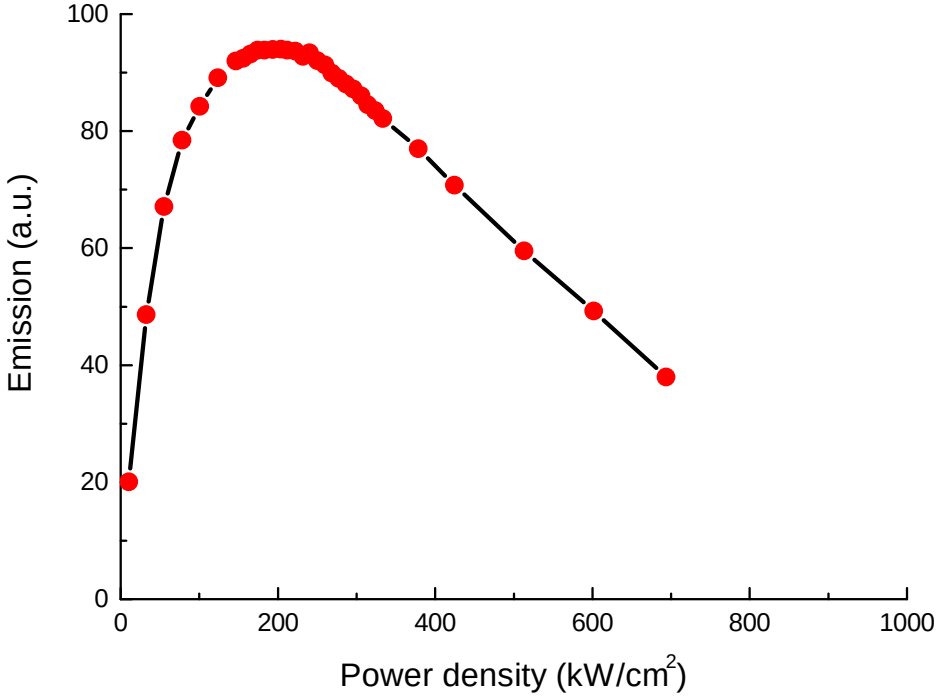

Figure 21: Emission dependence on power density for Y_2O_3:Yb,Er UCNPs under 980 nm CW pumping.

The behavior of the second type of UCNPs $NaYF_4$:Yb,Er with pump power density is different (Fig. 22). At low power density it also demonstrates the grow of luminescence emission. At the value 200 kW/cm^2, the emission reaches it maximum, and further increase of pump power density does not contribute to a significant increase in emission. Moreover, if the intensity of the incident light exceeds 900 kW/cm^2, a burnup of the nanoparticles occurs.

The causes of degradation and saturation are not obvious. A number of mechanisms can be responsible for these effects. One of them is related to the interaction of the activator and the sensitizer with the phonons of the host matrix crystal lattice. The peculiarity is that this interaction has both positive and negative contribution to the efficiency of upconversion luminescence. On the one hand, through the phonons, the

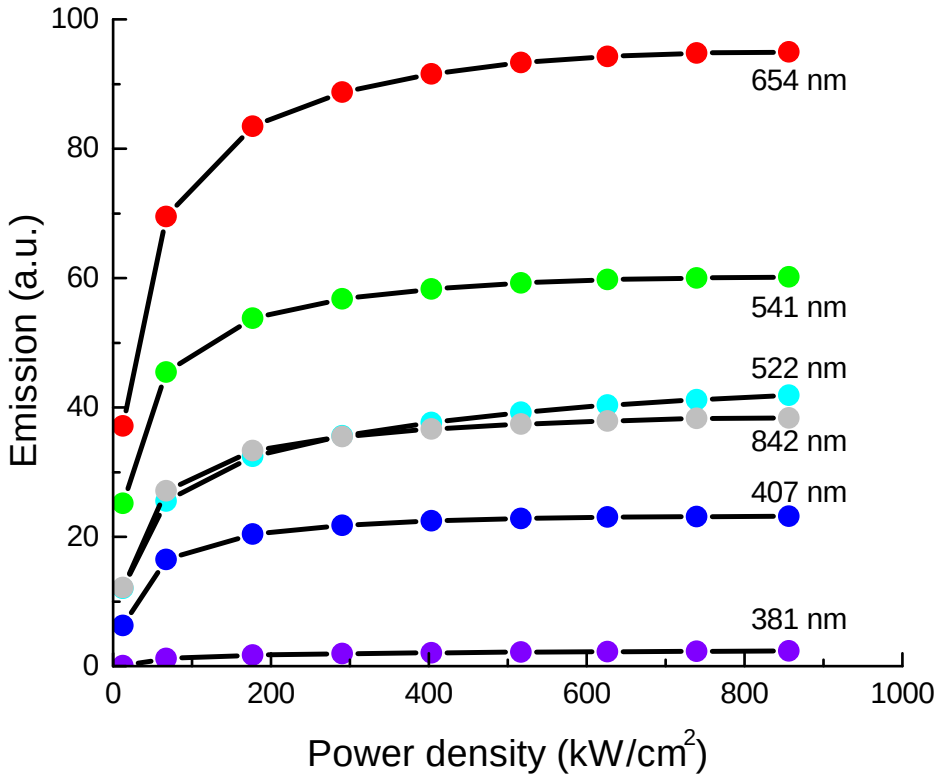

Figure 22: Emission dependence on power density for $NaYF_4$:Yb,Er UCNPs under 980 nm CW pumping.

sensitizer transfer to the activator the excess energy received from the photon, as described previously (see Fig. 4). On the other hand, non-radiative relaxation caused by phonons is the main reason for the decrease in the efficiency of the upconversion process [8]. Both these mechanisms are involved simultaneously in the upconversion processes. Up to a certain temperature, ytterbium efficiently transfers its excited energy to erbium, while the phonon-induced non-radiative decay is small. However, when the samples are heated up strongly, the vibrational energy of the host matrix crystal lattice increases to a level when non-radiative transitions begins to dominate. This leads to optical degradation, i.e. a decrease in the efficiency of the process, as shown in Fig. 21.

The first type of nanoparticles Y_2O_3:Yb,Er refers to oxides and is characterized by energy of phonons higher than the second type $NaYF_4$:Yb,Er, which is fluoride. The difference in the phonon energy could explain the phenomenon of degradation in the first case and the phenomenon of saturation in the second case. Since the phonon energy of the oxide is greater, non-radiative recombination associated with phonons is more intense than that of fluorides and outweighs the positive process of energy transfer from the sensitizer to the activator. In fluoride, where phonon energy is small, with an increase in temperature these two mechanisms are in balance, and saturation begins. To confirm this suggestion, an additional comprehensive and accurate measurements should be done. The external cooling of the samples down to optimal temperature

should be employed to avoid thermal heating effect in the upconversion process.

Second possible reason for optical degradation and saturation is light-induced structural changes. It can comprise as traps formation due to the oxygen vacancies, modification of nanoparticles surface or local structural changes surrounding the emitting sensitizer ions. To verify this suggestion, an additional structural measurements should be performed, such as fluorescence microscopy.

The spectra of nanoparticles contain several peaks in the visible range, so a triangular prism can be used to demonstrate the spectral composition of the upconversion luminescence.

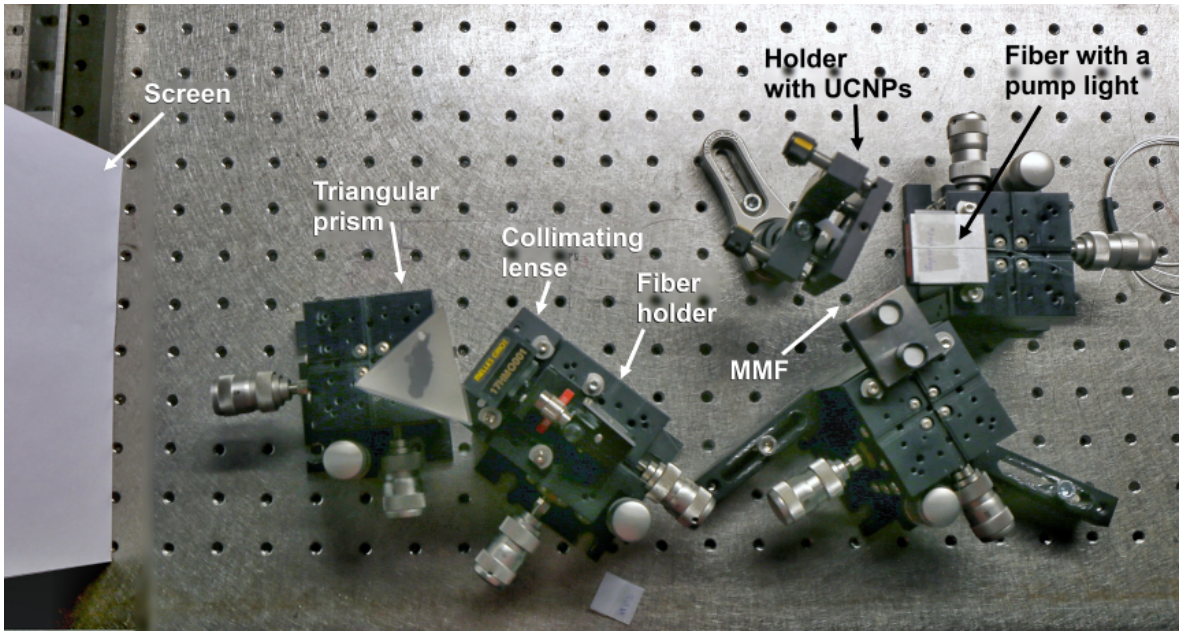

Figure 23: The scheme of spectrum decomposition using a triangular prism.

To simplify the scheme, the pumped fiber was set as close to the UCNPs as possible without any lens system (Fig. 23). A multimode fiber was used to collect emitted luminescence. At the output of the multimode fiber, the beam was collimated with a lens and directed to the prism. Due to the phenomenon of dispersion, the transmitted ray is spatially separated into components of different colors (different wavelengths). The result of decomposition is visible on a white screen in the form of spots of different colors (Fig. 24).

The spectra of luminescence of UCNPs for the 980 nm pulsed excitation are shown in Fig. 25 and 26. A comparison of the graphs 18, 19 and 25, 26 reveals no principal difference in the upconversion process under excitation by CW or pulse pumps. It means that the process is insensitive to the peak power (or pulse energy) of the pump, contrary to the opinion existing earlier, but rather it primarily determines by the power density: The higher power density of the pump, the more effective the upconversion process. The measured power density dependence under pulse pump

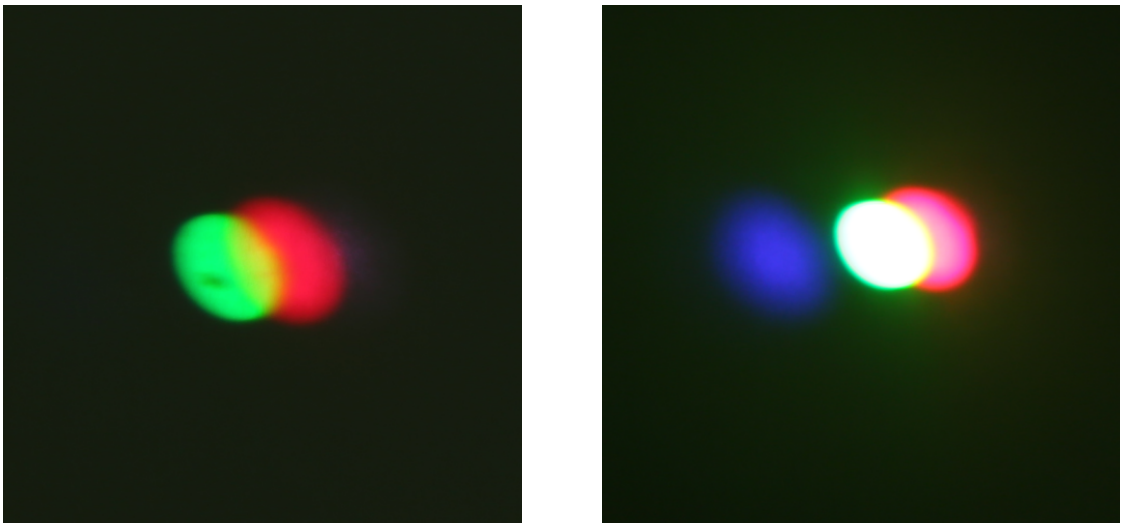

a) b)

Figure 24: Upconversion luminescence: a) Y_2O_3:Yb,Er, b) $NaYF_4$:Yb,Er UCNPs.

power excitation demonstrates also the tendency to the saturation in both UCNPs samples. However, the degradation or saturation effects was not reached.

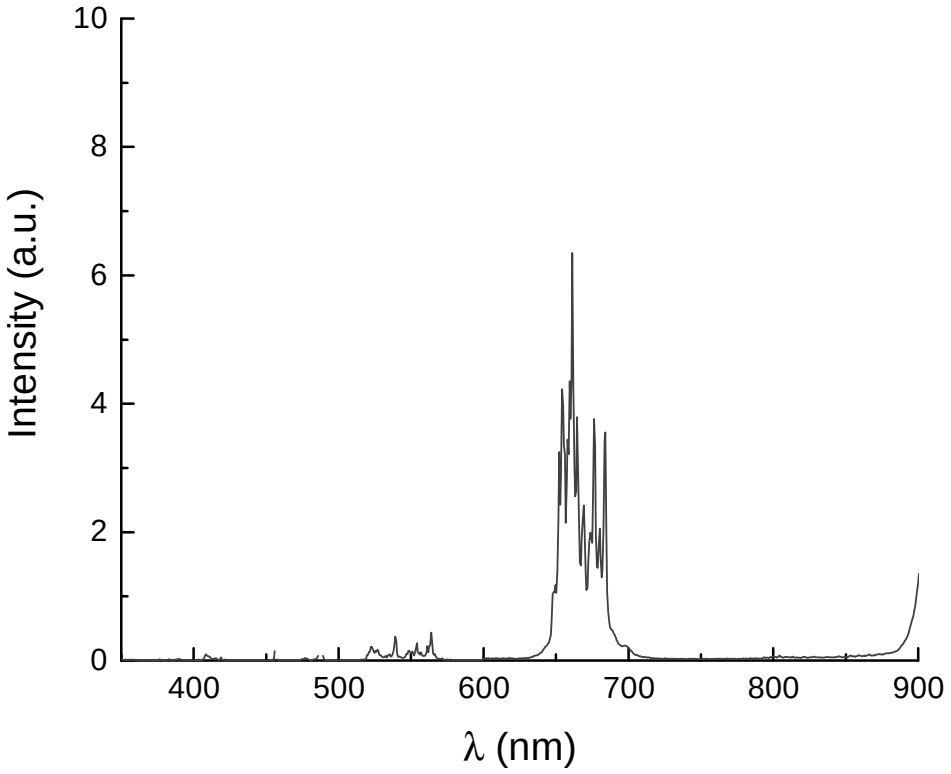

Figure 25: Spectrum of Y_2O_3:Yb,Er UCNPs within the range of 500 to 900 nm obtained under 980 nm CW pumping.

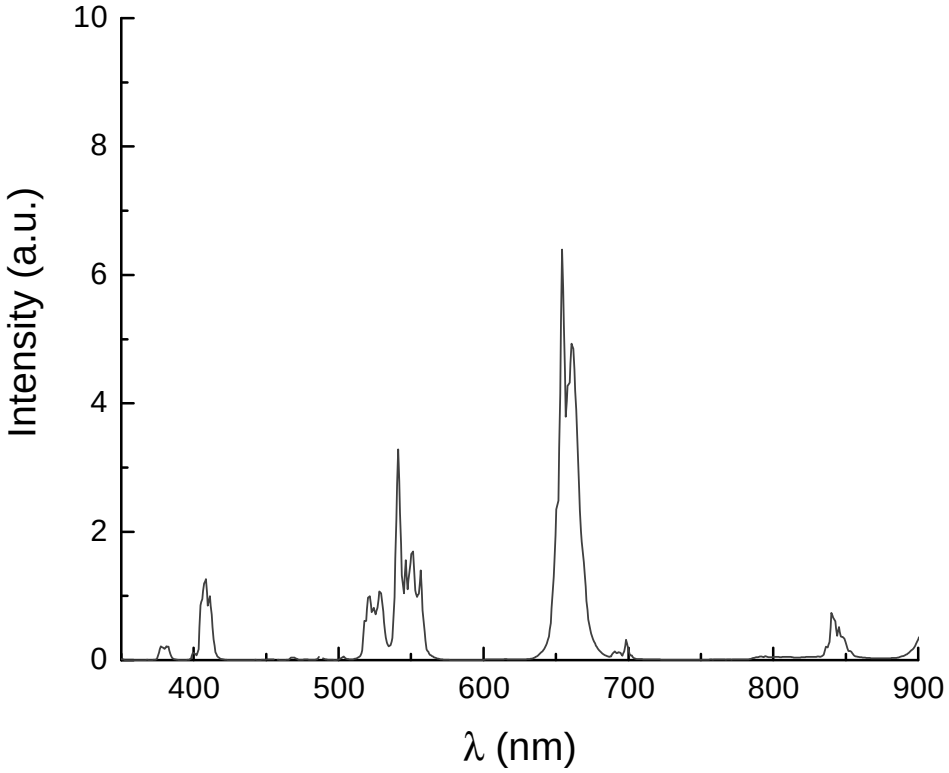

Figure 26: Spectrum of $NaYF_4$:Yb,Er UCNPs within the range of 350 to 900 nm obtained under 980 nm CW pumping.

In case of pulsed source irradiation of the UCNPs (Fig. 27 and 28) the heating effect of the sample is much lower than that with CW pumping. This is due to the reason that illumination happens occasionally during very short time (6 ps) and the material temperature rises slowly. In contrast, under CW pumping the excitation is disrupted resulting in a fast rise of the sample temperature.

The presence of the saturation effect tendency under pulse pumping denotes that the phonon-induced process could contribute in the degradation/saturation process, but it does not specify does it accompany by any other or not.

To investigate the principle possibility of degradation/saturation effect, the output power of the pulsed source should be rise to much higher level. It would require a second more powerful amplifier stage. A comparison of the samples temperatures under CW and pulsed pump sources, when the samples demonstrates unusual luminescence intensity dependence could give more information about the mechanisms involved in the upconversion process.

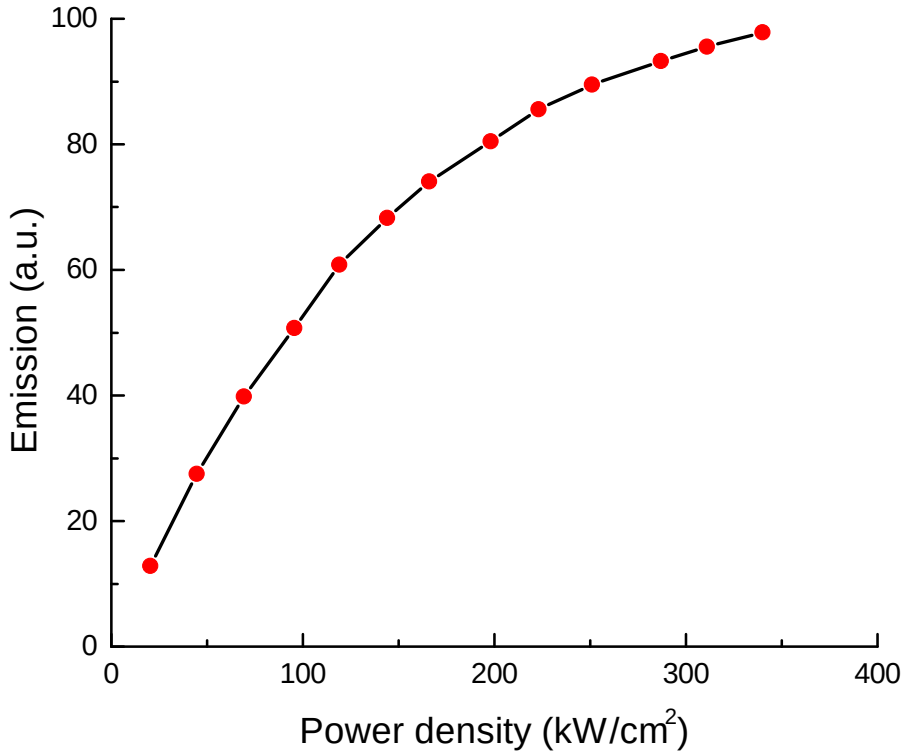

Figure 27: Emission dependence on power density for Y_2O_3:Yb,Er UCNPs under 980 nm pulsed pumping.

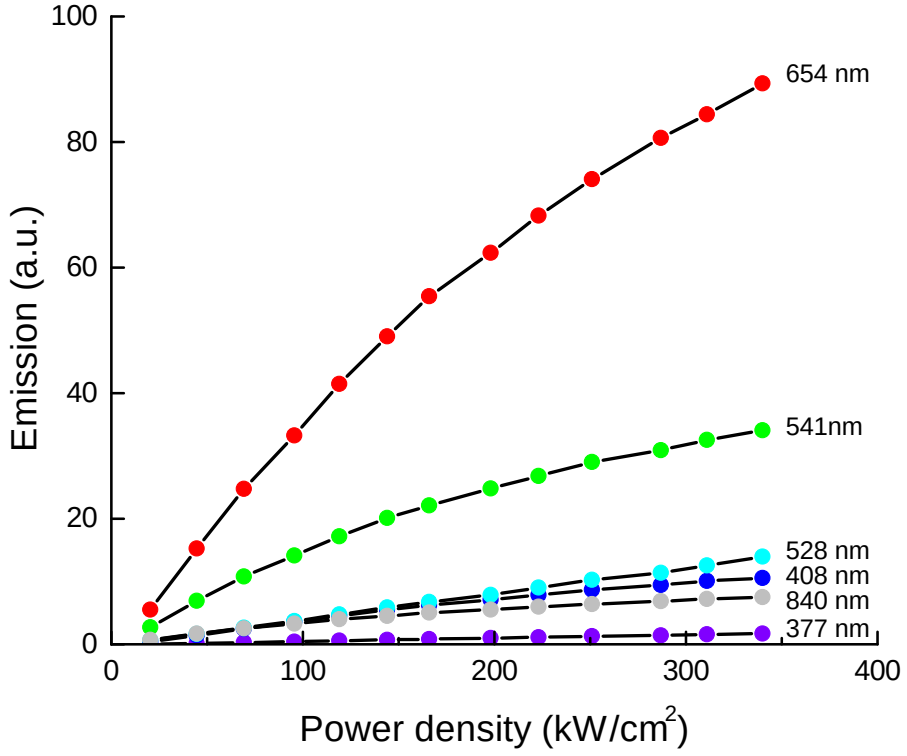

Figure 28: Emission dependence on power density for $NaYF_4$:Yb,Er UCNPs under 980 nm pulsed pumping.

As mentioned in Section 3.2, ytterbium has two peaks on the absorption spectrum. The first at 915 nm is broad and low, the second at 980 nm is narrow and high. Therefore, source at a wavelength of 915 nm can also be used for the pumping. Obtained spectrum of Y_2O_3:Yb,Er UCNPs under 915 nm CW pumping is depicted in Fig. 29.

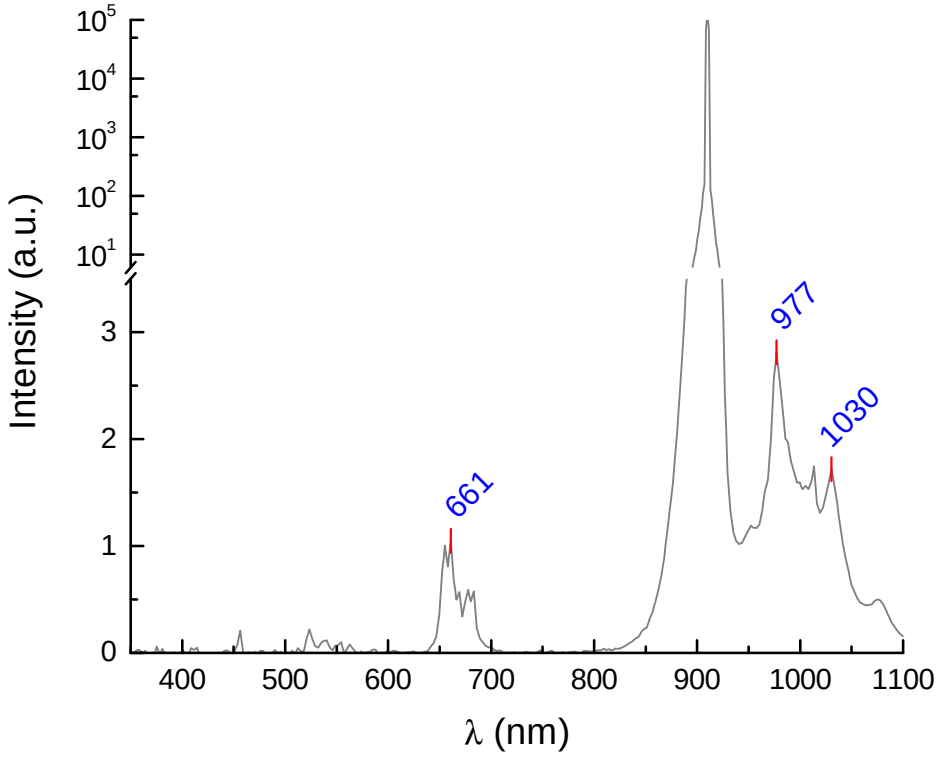

Figure 29: Spectrum of Y_2O_3:Yb,Er UCNPs under 915 nm CW pumping.

It contains peaks at 661, 915, 977 and 1030 nm. Huge peak at 915 nm is associated with unabsorbed pump light. The main feature of this spectrum is that the red upconversion peak at 661 nm is much smaller than downconversion peak at 977 nm. It means that energy transfer from ytterbium to erbium, which is responsible for 661 nm peak, is not effective. Ytterbium converts most of absorbed light y into radiation at 977 nm and 1030 nm, which takes place in Yb ions without energy transfer to Er-ions. Thus, under 915 nm pumping the donwconversion effect dominates and the cooperation between different ions is non-effecient.

6 Upconversion nanoparticles-doped coreless fibers

The utilization of nanoparticles powder is not convenient in terms of light collection since the nanoparticles emit within the whole hemisphere. In addition, the emitted light area is limited by beam size. Of course, it can be made as large as possible, but in this case it suffers from the power density which is the crucial parameters for upconversion processes as it was shown in Chapter 5. Therefore, the confinement of the UCNPs in the waveguide structure, where the pump light covers the whole area of nanoparticles, and it is delivered along the long side together with emitted light, could eliminate all disadvantages of the powder samples. In this point of view, the upconversion nanoparticles-doped fibers are considered as the best solution for efficient light conversion. In this section, the investigation of the luminescence of the world-first fiber doped by UCNPs are presented.

6.1 Fiber samples characterization

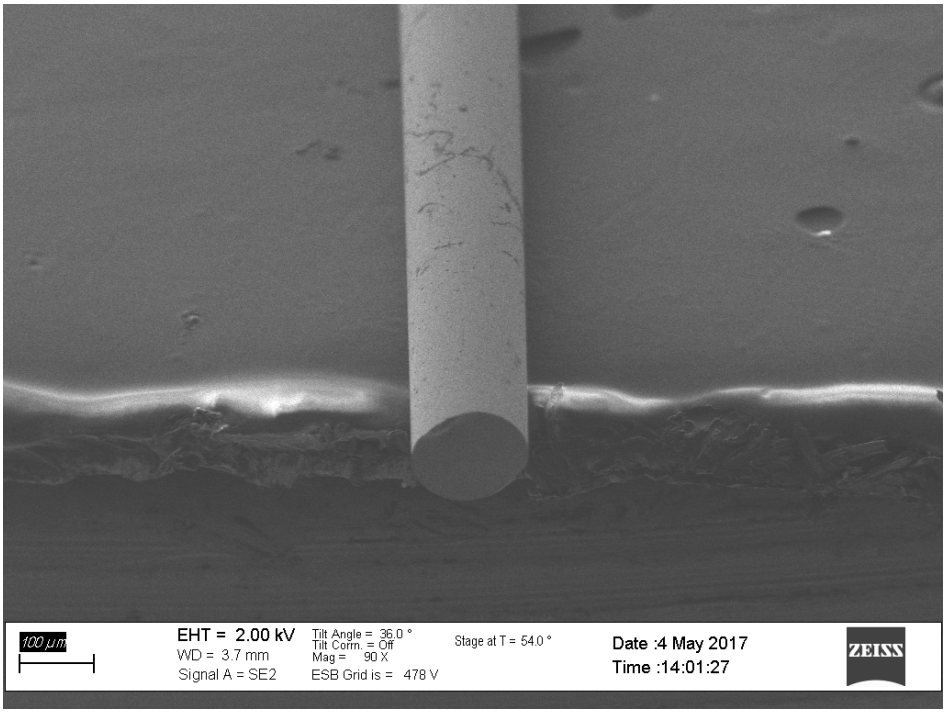

Figure 30: SEM image of UCNPs-doped fiber.

The world-first UCNPs-doped fibers were provided by University of Adelaide. They were made of tellurite-based glass and doped with $LiYF_4$:18%Yb,4%Er nanoparticles concentration of 70 ppm, which is 3 order of magnitude lower that usually Yb-Er-ions doped fiber concentration. For UCNPs, $LiYF_4$ compound was selected as the host matrix due to its low phonon energy ($\sim$566 cm^{-1}), thermal stability and reduced crystal strains. The fiber with a thickness of 162 microns (Fig. 30) has coreless structure and

does not contain the jacket. This is a typical case for the new type of fiber when the doping and fabrication technology are under initial stage of the development. The fiber, which is non-protected by the jacket, absorbs easily water from the air and becomes very fragile.

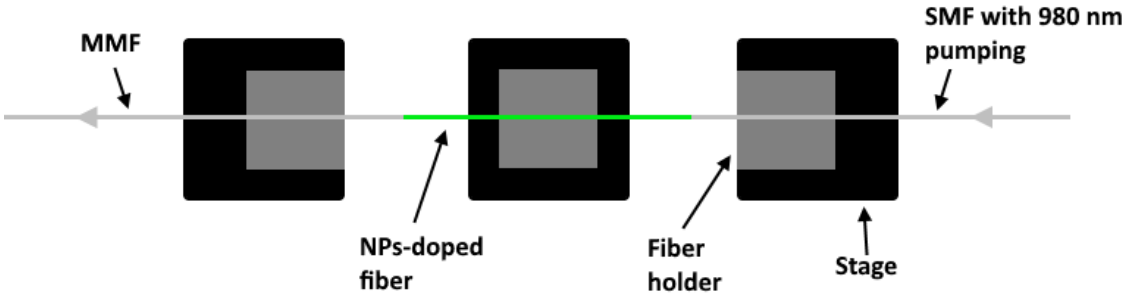

Figure 31: The scheme for pumping of NPs-doped fiber.

A fiber doped by upconversion nanoparticles was mounted on a fiber holder and fixed with an adhesive tape (conventional magnetic clamps were not used because of the extreme fragility of the fiber). The same CW laser diode II-VI LC96Z600-76 was used as a source of infrared light of 980 nm. Pump light was injected into the doped fiber directly without using any optics (Fig. 31). Fibers with length of 15 cm, were investigated for upconverion luminescence process.

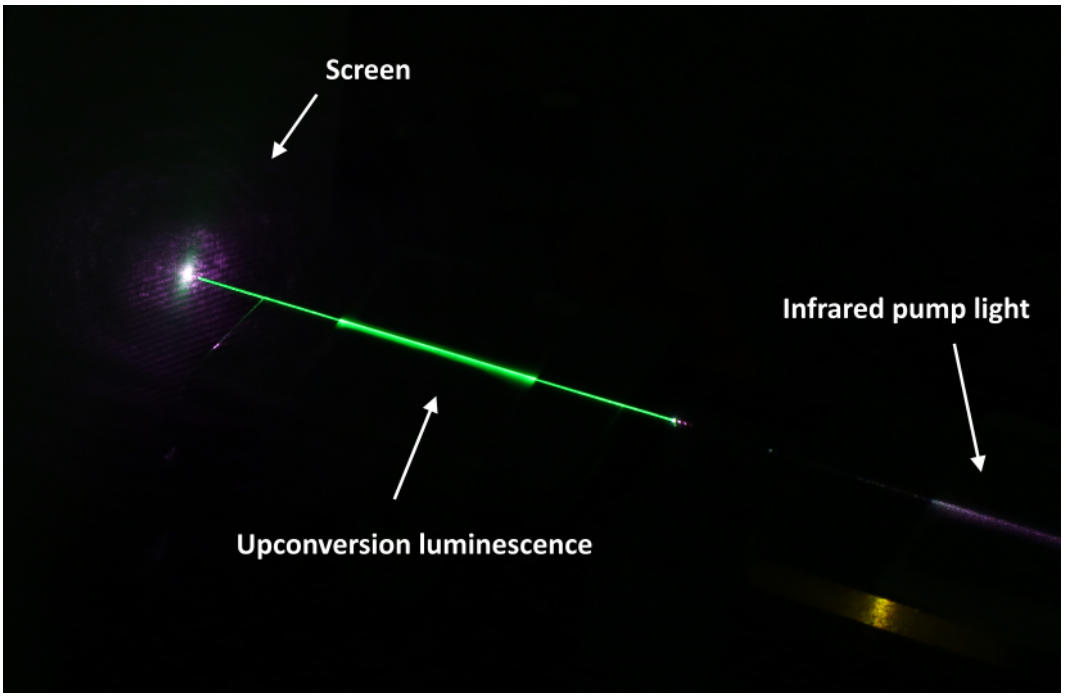

Figure 32: Photo of obtained upconversion luminescence in the world-first UCNPs fiber doped under pumping by 980 nm CW laser diode.

Upconversion luminescence at the wavelength of 550 nm, occuring in the fiber under the influence of infrared 980 nm pumping is shown in figures 32 and 33. The

brightness of the glow is not as high as in the case of UCNPs powder (Fig. 13), which indicates possible insufficient concentration of UCNPs in the fiber. Second reason for the reduction in efficiency of upconversion emission is that the investigated fiber is coreless, so the light propagation in such fiber is not as effective as in the structural fiber which has a core surrounded by a cladding, and characterizes by strong light confinement without scattering on the core/cladding surfaces impurities or dusts. In addition, as it was mentioned in the Section 4.4, the tellurite glass material is characterized by relatively high phonon energy 700 cm^{-1}, which also can negatively affect on the efficiency of the upconversion process.

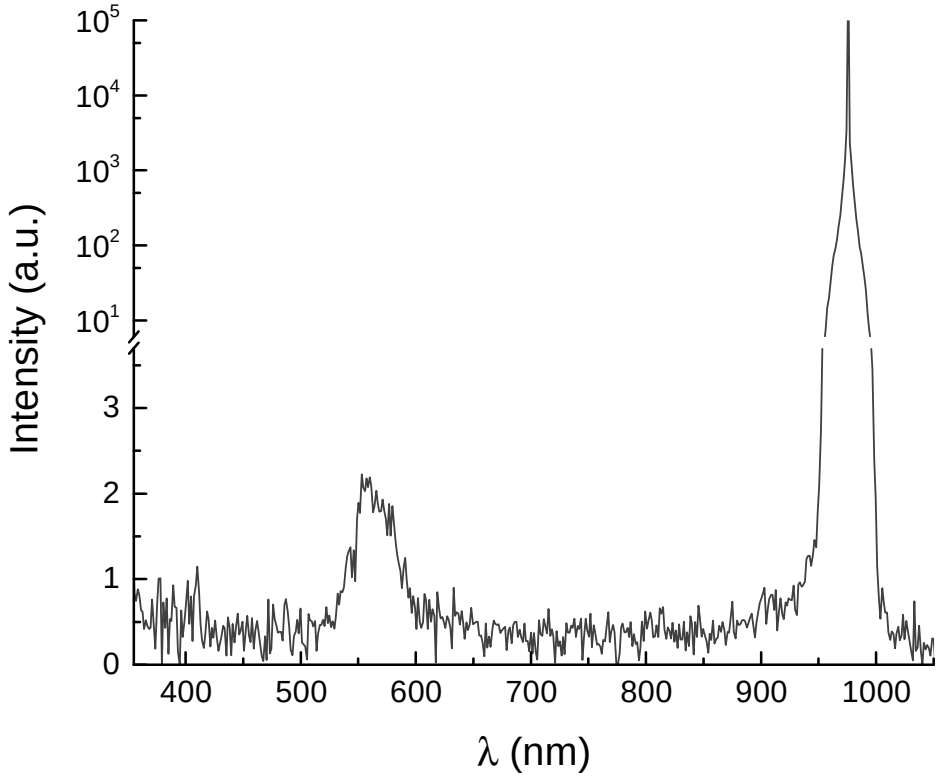

Figure 33: Luminescence spectrum of UCNPs-doped fiber.

A large amount of unabsorbed pumping light coming out of the doped fiber confirms the version that structure and doping level of the fiber is not optimal so far (Fig. 33). The UCNPs doping process in the glass material is very complicated. First, this is due to the fact, that nanoparticles size is in the order of several tens of nanometers, which is two orders of magnitude bigger, than conventional rare-earth ions have. This results in strong stresses in the glass matrix, which in its turn could lead to the high losses. In addition, there must be a critical balance in the case of the concentration of nanoparticles, since from a certain value, the nanoparticles start to form clusters inside the glass matrix, thereby, introduces the stresses and vacancies, which also have a negative impact on upconversion efficiency.

7 Conclusions

In this thesis, luminescent properties of upconversion nanoparticles were investigated. It was found that the spectrum of nanoparticles depends on the composition of the host matrix and the mass fraction of the lanthanides. Oxide-based UCNPs can be characterized as bicolor phosphor, since they emit red and green light. Fluoride-base UCNPs are multi-color, because their luminescence spectrum contains peaks in red, green, blue and violet portion of visible range.

Depending on the composition of the host matrix, with increasing pump power density, UCNPs exhibit effects of optical degradation and saturation. It can be assumed that the phonon-induced non-radiative transitions are responsible for these effects. However, other mechanisms are possible, therefore justification of the degradation and saturation effects requires additional measurements.

The excitation of nanoparticles by radiation at wavelength 980 nm showed its effectiveness in the upconversion luminescence processes. On the contrary, sources of 915 were not applicable for the excitation of Yb-doped upconversion nanoparticles, since Yb ions converts the pump light to strong emission at 980 nm and 1040 nm and most of the absorbed energy is expended on the downconversion process.

Studies carried out with the help of a scanning electron microscope and a transmission electron microscope made it possible to determine the size, shape, and structure of upconversion nanoparticles.

In addition, world-first optical fibers doped with upconversion nanoparticles were studied. Due to the insufficient concentration and structural features of the fiber, the upconversion luminescence in such fibers is observed at a low level. Since it is a completely new photonic material, the production technology requires adjustments. In particular, it is necessary to increase the concentration of UCNPs in the fiber for effective upconversion. But despite existing imperfection, the UCNPs-doped fibers represent the most convenient and promising form of UCNPs-containing material for the practical use.

The conducted studies revealed the main features in the properties of upconversion nanoparticles and determined the requirements for further research in this field.

References

[1] P. N. Prasad, *Nanophotonics*. Wiley, 2004.

[2] E. Yablonovitch, "Inhibited spontaneous emission in solid-state physics and electronics," *Phys. Rev. Lett.*, vol. 58, pp. 2059–2062, May 1987.

[3] S. John, "Strong localization of photons in certain disordered dielectric superlattices," *Phys. Rev. Lett.*, vol. 58, pp. 2486–2489, Jun 1987.

[4] F. Auzel, "Compteur quantique par transfert d'énergie entre deux ions de terres rares dans un tungstate mixte et dans un verre," *C. R. Acad. Sci.*, no. 262, pp. 1016–1019, 1966.

[5] F. Auzel, "Compteur quantique par transfert d'energie de Yb^{3+} à Tm^{3+} dans un tungstate mixte et dans un verre germanate," *C. R. Acad. Sci.*, no. 263, pp. 819–821, 1966.

[6] V. V. Ovsyankin and P. P. Feofilov, "Mechanism of summation of electronic excitations in activated crystals," *JETP Lett.*, vol. 3, no. 12, pp. 322–323, 1966.

[7] G. Chen, H. Qiu, P. N. Prasad, and X. Chen, "Upconversion nanoparticles: Design, nanochemistry, and applications in theranostics," *Chemical Reviews*, vol. 114, no. 10, pp. 5161–5214, 2014. PMID: 24605868.

[8] F. Zhang, *Photon Upconversion Nanomaterials*. Springer, 2015.

[9] L. Dong and B. Samson, *Fiber Lasers: Basics, Technology, and Applications*. CRC Press, 2016.

[10] J. S. Chivian, W. E. Case, and D. D. Eden, "The photon avalanche: A new phenomenon in Pr^{3+} based infrared quantum counters," *Applied Physics Letters*, vol. 35, no. 2, pp. 124–125, 1979.

[11] H. Yersin, *Transition Metal and Rare Earth Compounds. Excited States, Transitions, Interactions II*. Springer-Verlag Berlin Heidelberg, 2001.

[12] A. F. El-Sherif and M. K. El-Tahlawy, "Design and performance analysis of a tunable and self-pulsation diode pumped double-clad d-shaped Yb^{3+}-doped silica fiber laser," *Optical Engineering*, vol. 50, no. 4, pp. 044201–044201–8, 2011.

[13] F. Wang and X. Liu, "Upconversion multicolor fine-tuning: Visible to near-infrared emission from lanthanide-doped $NaYF_4$ nanoparticles," *Journal of the American Chemical Society*, vol. 130, no. 17, pp. 5642–5643, 2008.

[14] H. Zhang, Y. Li, Y. Lin, Y. Huang, and X. Duan, "Composition tuning the upconversion emission in $NaYF_4$:Yb/Tm hexaplate nanocrystals," *Nanoscale*, vol. 3, pp. 963–966, 2011.

[15] L. Tian, Z. Xu, S. Zhao, Y. Cui, Z. Liang, J. Zhang, and X. Xu, "The upconversion luminescence of $Er^{3+}/Yb^{3+}/Nd^{3+}$ triply-doped β-$NaYF_4$ nanocrystals under 808-nm excitation," *Materials*, vol. 7, no. 11, pp. 7289–7303, 2014.

[16] N. Menyuk, K. Dwight, and J. Pierce, "NaYF4:Yb,Er – an efficient upconversion phosphor," *Applied Physics Letters*, vol. 21, no. 4, pp. 159–161, 1972.

[17] K. W. Krämer, D. Biner, G. Frei, H. U. Güdel, M. P. Hehlen, and S. R. Lüthi, "Hexagonal sodium yttrium fluoride based green and blue emitting upconversion phosphors," *Chemistry of Materials*, vol. 16, no. 7, pp. 1244–1251, 2004.

[18] S. Lahtinen, A. Lyytikäinen, H. Päkkilä, E. Hömppi, N. Perälä, M. Lastusaari, and T. Soukka, "Disintegration of hexagonal $NaYF_4$:Yb^{3+},Er^{3+} upconverting nanoparticles in aqueous media: The role of fluoride in solubility equilibrium," *The Journal of Physical Chemistry C*, vol. 121, pp. 656–665, jan 2017.

[19] J.-C. Boyer, L. A. Cuccia, and J. A. Capobianco, "Synthesis of colloidal upconverting $NaYF_4$:Er^{3+}/Yb^{3+} and Tm^{3+}/Yb^{3+} monodisperse nanocrystals," *Nano Letters*, vol. 7, no. 3, pp. 847–852, 2007. PMID: 17302461.

[20] G. Chen, H. Qiu, R. Fan, S. Hao, S. Tan, C. Yang, and G. Han, "Lanthanide-doped ultrasmall yttrium fluoride nanoparticles with enhanced multicolor upconversion photoluminescence," *J. Mater. Chem.*, vol. 22, pp. 20190–20196, 2012.

[21] D. Bailey and E. Wright, *Practical Fiber Optics*. Elsevier, 2003.

[22] J. M. Senior and M. Y. Jamro, *Optical fiber communications: principles and practice*. Financial Times/Prentice Hall, 2009.

[23] I. A. Sukhoivanov and I. V. Guryev, *Photonic crystals: physics and practical modeling*. Springer, 2009.

[24] G. P. Agrawal, *Fiber-optic communication systems*. Wiley, 2010.

[25] E. Desurvire, J. L. Zyskind, and C. R. Giles, "Design optimization for efficient erbium-doped fiber amplifiers," *Journal of Lightwave Technology*, vol. 8, pp. 1730–1741, Nov 1990.

[26] M. J. Digonnet, *Rare-Earth-Doped Fiber Lasers and Amplifiers, Revised and Expanded*. Optical Science and Engineering, CRC Press, 2nd ed., 2001.

[27] L. Skuja, M. Hirano, H. Hosono, and K. Kajihara, "Defects in oxide glasses," *physica status solidi (c)*, vol. 2, no. 1, pp. 15–24, 2005.

[28] W. F. Krupke and J. B. Gruber, "Absorption and fluorescence spectra of $Er^{3+}(4f^{11})$ in LaF_3," *The Journal of Chemical Physics*, vol. 39, no. 4, pp. 1024–1030, 1963.

[29] W. T. Carnall, G. L. Goodman, K. Rajnak, and R. S. Rana, "A systematic analysis of the spectra of the lanthanides doped into single crystal LaF_3," *The Journal of Chemical Physics*, vol. 90, no. 7, pp. 3443–3457, 1989.

[30] G. H. Dieke and H. M. Crosswhite, "The spectra of the doubly and triply ionized rare earths," *Appl. Opt.*, vol. 2, pp. 675–686, Jul 1963.

[31] Y. Liu, Y. Lu, X. Yang, X. Zheng, S. Wen, F. Wang, X. Vidal, J. Zhao, D. Liu, Z. Zhou, C. Ma, J. Zhou, J. A. Piper, P. Xi, and D. Jin, "Amplified stimulated emission in upconversion nanoparticles for super-resolution nanoscopy," *Nature*, vol. 543, pp. 229–233, Mar 2017.